Revalorization of barley straw and husk as precursors for cellulose nanocrystals extraction and their effect on PVA_CH nanocomposites

E. Fortunati[a*], P. Benincasa[b], G.M. Balestra[c], F. Luzi[a], A. Mazzaglia[c], D. Del Buono[b], D. Puglia[a], L. Torre[a]

[a]*University of Perugia, Civil and Environmental Engineering Department, UdR INSTM, Strada di Pentima 4, 05100 Terni (Italy)*

[b]*University of Perugia, Department of Agricultural, Food and Environmental Sciences, Borgo XX Giugno 74, 06121 Perugia (Italy)*

[c]*University of Tuscia, Department of Sciences for Agriculture and Forestry (DAFNE), Via S. Camillo de Lellis sns, 0100 Viterbo (Italy)*

[*]**Corresponding author**: Tel.: +39-0744492921; fax: +39-0744492950; E-mail address: elena.fortunati@unipg.it (E. Fortunati)

Abstract

Poly(vinyl alcohol) (PVA) blended with natural chitosan (CH) was selected as matrix for the production, by solvent casting in water, of nanocomposite films containing cellulose nanocrystals (CNC) extracted from barley residues, that were introduced in PVA_CH systems as reinforcement phases. Cellulose nanocrystals were successfully extracted from both barley straw and husk by applying two different approaches, a chemical alkaline and an enzymatic pre-treatment, followed by acidic hydrolysis. The results evidenced the major effectiveness of the enzymatic pre-treatment on the quality of obtained CNC; nevertheless, all the different typologies of nanocrystals were added to the polymers and the morphological, optical, mechanical response, thermal and migration characteristics were investigated, whereas antimicrobial assay were carried out to evaluate the bactericidal effect induced by chitosan presence. The results indicated that chitosan reduced the optical transparency and the mechanical response of PVA matrix, whereas its combination with

CNC (especially when extracted by enzymatic treatment and added at a higher content) was able to modulate the optical properties, the mechanical and thermal responses. Moreover, inhibitions on fungal and bacterial development were detected for PVA_CH_CNC ternary systems, suggesting their protective function against microorganisms contamination.

Keywords: barley crop residues, cellulose, chemical pre-treatment, enzymatic pre-treatment, nanocomposites, antibacterial.

1. Introduction

In the last years there was a general interest in the sustainable production of materials from wastes, since the use of agricultural and food technology residues, both for the preparation of biopolymers and extraction/synthesis of nanostructured materials, is attractive from technical and environmental points of view (Dhar et al., 2014; Li, Mascheroni and Piergiovanni, 2015; Mohammadinejad et al,. 2016). Furthermore, some disadvantages of biopolymers, such as weak mechanical and barrier properties, can be significantly reduced by the use of nanocellulose (Khan et al., 2014), while these materials can also be used as carriers for specific active ingredients (antioxidants and antimicrobials). Looking at this specific application, a plethora of examples can be found in the literature on the extraction of different cellulosic nanostructures from agro-waste sources. In particular, diverse chemical/biochemical and mechanical procedures have been previously applied in order to obtain nanocellulose; in spite of this, it should be pointed out that the morphology of nanocellulose is mainly depending on both the fibre sources and biomass processing. To date, many agricultural by-products are being used to isolate cellulose fibrils while nanocellulose production using cereal by-products such as wheat straw, soy hulls (Alemdar and Sain, 2008), soybean straw (Reddy and Yang, 2009) and rice straw (Lu and Hsieh, 2012b), bagasse (de Campos et al., 2013), cornhusk (Reddy and Yang, 2005), grape hulls (Lu and Hsieh, 2012a) and also barley straw and

husk (Espino et al., 2014; Sun et al, 2005) has been investigated. In this context, it is important to underline that grain barley is the fourth most widespread cereal in the world, with a total acreage of about 50 million hectares and a total grain production of about 150 million tons, of which about 40% in the EU, 20% in Eastern Europe, 10% in Northern America, the remainder mainly in temperate regions of the other continents. Grain barley is mainly used as animal feed and for malting and brewing. Barley straw, i.e. the crop residues remaining in the field after grain harvest, has a very high C/N ratio, which limits its contribution to soil humus restoration and can even cause temporary N deficiency to the following crop (Wessén and Berg, 1986). Barley grain is generally husked. Whereas in animal feed, barley husks are eaten and digested, in brewing they represent a by-product. Both straw and husk have been proposed as thermal-electric power sources (Singh, 2015) or as components for bio-based materials (Bowyer and Stockmann, 2001) with several recognized properties as, for example, thermal insulation (Palumbo, Avellaneda and Lacasta, 2015). In alternative, since they contain relevant amounts of cellulose (Adapa et al., 2009; Sun et al., 2005), they have been proposed for cellulose extraction (Sun et al.,2005) or isolation of cellulose nanocrystals (CNC) by acid hydrolysis (Espino et al., 2014). In particular, CNC can be recovered from lignocellulosic wastes (or materials of scarce value) by carrying out, as a first step, the removal and cleaning of cellulose from the other fibres. In the second step, the purified polymeric carbohydrate can be chemically transformed into nanocrystals of cellulose. Therefore, the first step regards the purification of fibres from pectin, lignin and hemicelluloses, which are strongly linked and interconnected with cellulose (Pakarinen et al., 2012), and are the main interfering to the cellulose purification procedures. In fact, these compounds, if remaining in high amounts in the derived matrices, can negatively affect the quality of the final nanocomposite materials. In order to disassemble the lignocellulosic materials, without losing the desired carbohydrate, the complex interactions of cellulose with the other fibres are to be solved (Korte and Staiger, 2008). To this purpose, the starting materials can be subjected to some different pre-treatments (Pakarinen et al., 2012), which, basically, can be grouped into chemical or enzymatic pre-treatments. After these pre-

80 treatments, the successive and final step carried out in order to convert the cellulose in nanocrystals
81 is an acidic hydrolysis (Bondeson et al., 2006). This last step is general, of value and based on the
82 use of sulfuric acid, while some different chemical and enzymatic strategies can be applied to the
83 raw materials in order to purify and extract cellulose. In particular, a very common way to eliminate
84 the interfering substance from cellulose is the alkaline pre-treatment of the lignocellulosic materials
85 (Li and Pickering. 2008). Instead of its aggressive nature and some environmental issues associated
86 with this type of pre-treatment, the use of alkali permits to achieve good result, characterized by
87 satisfying yields (Luzi et al., 2014). As examples of the efficacy of this chemical pretreatment,
88 some authors showed how this treatment can be particularly adequate in eliminating the major part
89 of pectin and lignin in hemp fibres (Wang, et al., 2003; Luzi et al., 2014). On the other hand, the
90 more recent technology based on the use of hydrolytic enzymes, in combination or not with some
91 organic chelating compounds, is becoming a very popular approach to pre-treat the lignocellulosic
92 materials, with the aim to purify the cellulose from the other interfering compounds, prior to its
93 final acidic hydrolysis to give CNC (Li and Pickering. 2008). The enzymatic pre-treatments are
94 more specific than the chemical ones and less impacting on the environment (Siqueira et al., 2010).
95 To this regard, the use of pectinases and cellulases has attracted noticeable attention for their
96 efficacy in removing water-extractives, minerals, pectins and amorphous hemicelluloses (Siqueira
97 et al., 2010).
98 Although barley straw and husk were recently used for cellulose nanocrystals production (Espino et
99 al., 2014; Sunm et al., 2005), to date, there are no literature reports addressing the question whether
100 these cellulosic sources can be used for realizing polymeric matrices suitable for food packaging
101 applications. To this regard, it is well know that the hydrophilic surface of CNC allows appropriate
102 blending with water-soluble polymer matrices such as poly(vinyl alcohol) and chitosan. Chitosan
103 blended with PVA has been investigated demonstrating good mechanical and chemical properties
104 (Nakano et al. 2007). Moreover, the incorporation of a multifunctional nanosized filler such as CNC
105 would be expected to modulate the mechanical properties, ultraviolet-absorbing ability and

106 antibacterial activity in a nanocomposites approach. Cellulose nanocrystals from different sources
107 were incorporated, by using different methods, both in PVA (Fortunati et al. 2013; Zhang et al.,
108 2014) and chitosan polymeric matrices (Khan et al., 2012; Li et al. 2013) separately, whereas the
109 incorporation in PVA/CH blends was reported by few authors. El Miri et al. studied the effect of the
110 introduction of CNC isolated from sugarcane bagasse (El Miri et al., 2015) in a PVA/CH (50:50)
111 blend. The authors proved that strong electrostatic interactions and numerous hydrogen bonding
112 between hydroxyl groups and anionic sulfate groups of CNC or the amine groups of the PVA/CH
113 polymeric blend, ensured high compatibility between the CNC and the nanocomposite films. Li et
114 al (Li et al., 2015) used cellulose nanowhiskers (CNW) from ramie and demonstrated that
115 antimicrobial and oxygen barrier properties of the nanocomposites were positively improved
116 making the nanocomposites potentially useful for many applications.
117 In this context, the main goal of this research was the use of barley straw and husks as sources of
118 cellulose nanocrystals (CNC). To this purpose, two procedures for cellulose purification were
119 developed (chemical and enzymatic pre-treatments) and compared, with the objective to guarantee
120 the sustainability of the applied techniques. Furthermore, the potential of CNC, extracted from
121 straw and husk, by applying both the above two pre-treatments, as reinforcement phases in
122 multifunctional nanocomposite films based on PVA_CH blend were here extensively analysed and
123 deeply discussed.
124

125 **2. Experimental Part**

126 **2.1. Materials**

127 Barley straw and husk were collected from the malting barley cultivar Quench grown at the
128 Experimental Station of the Department of Agricultural, Food and Environmental Sciences, located
129 near Papiano (Perugia Province), a plain land of the middle Tiber Valley (165 m asl, 42°57' N
130 12°20″E) in Central Italy. The crop was sown on November 27, 2014 at a density of 350 seeds m^{-2}
131 and harvested on June 23, 2015, yielding over 8 Mg of grains ha^{-1} and thus, roughly, a similar

amount of straw. Straw samples were collected and finely grinded. Grains were de-husked mechanically and the husk was first separated from grain residues by air flow and then finely grinded. The grinding of straw and husk was carried out avoiding heating.

All chemicals and reagents, including toluene, ethanol, sodium hydroxide (NaOH, reagent grade ≥98 %), sodium chlorite ($NaClO_2$, puriss p.a. 80%), acetic acid (CH_3COOH) and sodium bisulfate ($NaHSO_4$, purum, anhydrous, ~95.0%) were supplied by Sigma-Aldrich®(Milan, Italy).

Pectinase and Cellulase from *Apergillus niger* were supplied by Sigma-Aldrich® (Milan, Italy).Polymer matrices, poly(vinyl alcohol) (PVA, average Mw 124-146 Kg mol^{-1}, 99% hydrolyzed), and high molecular weight chitosan (CH) (degree of deacetylation:75-85%, viscosity: 200-800 cPs),were supplied by Sigma-Aldrich® (Milan, Italy).

2.1.1. Raw material composition

Dry weight, ashes and lipids contents of barley straw and husk were determined according to the official Italian Analytical Methods and they are presented in Table 1.

Protein contents of straw and husk were determined according to Kjeldahl (1883). Briefly, 0.5 g of dry weight samples were acid digested with H_2SO_4 96% and H_2O_2 (30 v/v%) and one Kjeldahl tablet. Tubes were boiled and, after cooling, NaOH 32.5 (w/v) % was added. The protein content was then evaluated by titration (Kjeldahl, 1883).

Cellulose, hemicellulose, lignin, pectin contents were determined according to Van Soest (1963) (Van Soest, 1963).

2.2.Chemical pre-treatment of barley straw and husk

Barley straw and husk were chemically pre-treated following two different procedures (Scheme 1), according to the characteristics of the raw materials used as precursors.

Pre-Treatment of barley straw: Firstly, barley straw fibres were washed several times with distilled water and then dried at room temperature (RT). Subsequently, fibres were chopped to an

158 approximate length of 5-10 mm, and de-waxed by boiling them in a mixture toluene/ethanol (2:1
159 v/v) for 6 h. The fibres were then filtered, washed with ethanol for 30 min and dried. Afterwards, a
160 treatment based on a bleaching process was applied twice to this matrix for the cellulose extraction.
161 Briefly, barley straw was initially treated with sodium chlorite ($NaClO_2$) 0.7 (wt/v)%, then the
162 fibres (liquor ratio 1:50) were boiled for 2 h and the pH of the solution was lowered to about 4 by
163 means of acetic acid. Finally, the material was treated with sodium hydroxide (NaOH) 17.5 (wt/v)
164 % at RT for 20 minutes, filtered and washed with distilled water.
165 *Pre-Treatment of barley husk:* barley husk were initially washed with distilled water to remove the
166 impurities, which envelop the external surface of fibre cell walls. The fibres were dried at RT and
167 then treated (liquor ratio 1:50) two times, before bleaching, with a NaOH 4 (wt/v) % for 2 h at 100
168 °C under mechanical stirring. Afterwards, the solid residue was washed several times with distilled
169 water until neutrality was reached (Johar et al., 2012). Thereafter, the bleaching process was
170 repeated two times by using a buffer solution of acetic acid (pH about 4), containing $NaClO_2$ 1.7
171 (wt/v) % under magnetic stirrer. The fibres (liquor ratio 1:50) were then boiled for 2 h (Henrique et
172 al., 2013; Johar et al., 2012), washed with distilled water and finally dried at RT.
173 For both the applied procedures the final yield was calculated as % of initial weight of the used raw
174 material.
175

176 **2.3. Enzymatic pre-treatment of barley straw and husk**

177 Cellulose was extracted from barley husk and straw by combining some alkaline washing with
178 enzymatic digestions, in order to progressively remove the unwanted compounds (lignin, pectin and
179 hemicelluloses). To this purpose, straw was chopped to 1 cm length and then grinded. On the other
180 hand, husk was not grinded in order to avoid excessive warming, but immediately submitted to the
181 extraction procedure. Straw powder and husk (100 g) were washed twice with distilled water (1:5
182 wt/v). Afterwards, dripped matrices were repeatedly treated with an aqueous solution of NaOH 5
183 (wt/v)% for 1 hour with vigorous stirring, until the liquid phase was colorless. Solid residues were

184 then filtered under vacuum, washed again with water and finally autoclaved in 1L of distilled water
185 (120 °C and 1.5 atm) for 1 hour. After that, the suspensions were filtered and the solid residues
186 collected, treated for 1 hour with an aqueous solution of NaOH (2 (wt/v)%) and left to dry overnight
187 at 60 °C. Dried residues were then re-suspended in 1 L of a buffer solution (citrate 50 mM, pH 4.3)
188 and incubated with pectinase from *Apergillus niger* (5000 U – Sigma-Aldrich) for 24 hours at 45°C.
189 Successively, the suspension was rapidly heated until boiling and so maintained for 10 minutes. The
190 suspension was newly filtered and the solid residues re-suspended in 1 L of the citrate buffer and
191 added of a cellulase from *Aspergillus niger* (5000 U – Sigma-Aldrich). Then, the mixture was left to
192 incubate for 24 hours at 45°C. The suspension was boiled for 10 minutes and the solid residue was
193 recovered for filtration, treated with 300 mL 0.2 (v/v) % sodium hypochlorite, for the final
194 blanching, filtered and dried at 60 °C for 2 days. The final yield was calculated, also in this case, as
195 % of initial weight of the used raw material.
196
197 **2.4. Characterization of pre-treated barley straw and husk**
198 The microstructure, dimension and appearance of raw materials, and chemically and enzymatically
199 pre-treated barley wastes (obtained from straw and husk), were investigated by field emission
200 scanning electron microscope (FESEM, Supra 25-Zeiss). The fibres were prepared as previous
201 reported (Fortunati et al., 2016). FESEM images of the fibres were analyzed by Image J software in
202 order to determine the dimensions of the studied materials.
203 Fourier infrared (FTIR) spectra of raw materials and chemically and enzymatically pre-treated
204 barley wastes were recorded using a Jasco FTIR 615 spectrometer in the 400–4.000 cm^{-1} range, in
205 transmission mode. The fibres were analyzed by means of KBr discs made by using pulverized
206 fibres and dust of KBr.
207 Finally, thermogravimetric measurements (TGA) were performed by using a Seiko Exstar 6300
208 analyzer using an heating scan from 30 to 900 °C at 10 °C min^{-1} in nitrogen atmosphere.
209

2.5. Cellulose nanocrystal extraction and characterization

Cellulose nanocrystals were obtained by acidic hydrolysis of the chemically (designed as CNC_{straw_chem} and CNC_{husk_chem}) or enzymatically (designed as CNC_{straw_enz} and CNC_{husk_enz}) pre-treated barley straw and husks (Fortunati et al., 2013; Luzi et al., 2014). In detail, the hydrolysis was carried out with 64 (wt/wt)% sulfuric acid at 45 °C for 30 min. Then, the cellulose suspension was centrifuged and dialyzed, prior to its addition for 48 h to a mixed bed ion exchange resin (Dowex Marathon MR-3 hydrogen and hydroxide form). The resultant cellulose nanocrystal aqueous suspension was ultrasonicated by means of a tip sonicator (Vibracell, 750) for 5 min. The final dry-content of different extracted CNC in aqueous solution ranged from 0.4 (wt/wt)% and 0.9 (wt/wt)% and the reaction yield after the hydrolysis was calculated as % of initial weight of the used pre-treated fibres.

The microstructure of obtained CNC_{straw_chem}, CNC_{husk_chem} and CNC_{straw_enz} and CNC_{husk_enz}, was investigated by FESEM. Fourier infrared (FTIR) spectra of freeze-dried CNC were recorded in transmission mode using KBr discs, whereas thermogravimetric measurements were performed using a heating scan from 30 to 900 °C at 10 °C min^{-1} in nitrogen atmosphere.

The crystallinity of cellulose nanocrystals, obtained by means of the acidic hydrolysis of straw and husk fibres chemically or enzymatically pre-treated, was determined by X-ray diffraction method. X-ray diffraction patterns were collected with a Philips X'Pert PRO MPD diffractometer operating at 40 kV and 40 mA, with a step size of 0.0167 and 20 s counting time, in the 4-60 ° 2-theta range, using Cu Ka radiation and an X'Celerator detector.

2.6. PVA_CH based nanocomposite films

2.6.1. PVA_CH nanocomposite preparation

PVA_CH blend films were prepared dissolving PVA in deionized water at 5 (wt/v) % under magnetic stirring at 90 °C for 4 h, and chitosan (0.15 (wt/wt)%) in water with glacial acetic acid (1 (v/v)%) under magnetic stirring at 40 °C for 12 h. The solution of chitosan was mixed (ratio of CH

10 (wt)%) with the PVA (ratio of PVA 90 (wt)%) solution and sonicated (Vibracell 75043, 750W, Bioblock Scientific) for 5 min at 40% of amplitude. The obtained homogeneous PVA_CH solutions were poured into a Petri dish cover by a *Teflon*® sheet and dried in an oven at 40°C for 24-48 h.

PVA_CH based nanocomposite films reinforced with CNC extracted both chemically and enzymatically from barley straw and husk ,were prepared with the same procedure described above. Firstly, all the typologies of CNC (CNC_{straw_chem}, CNC_{husk_chem} and CNC_{straw_enz} and CNC_{husk_enz}) were added at 1 wt% to the PVA and PVA_CH solutions, sonicated for 2 min at 40% of amplitude, casted onto a Petri dish covered by a *Teflon*®, and dried. Then, on the basis of the results obtained from the different characterizations carried out on the nanocomposites loaded with 1 %wt of CNC, a higher content (3 %wt) of nanofillers extracted by means of the enzymatic pre-treatment, followed by acidic hydrolysis (CNC_{straw_enz} and CNC_{husk_enz}), was considered. All the produced formulations are summarized in Table S1 and PVA neat film was also produced for comparison. PVA_CH_CNC based films (50±5) μm thick were obtained. The films were equilibrated in desiccators for 1 week after processing and before the tests.

2.6.2. Characterization of PVA_CH nanocomposite films

The microstructure of the PVA_CH_CNC fractured surfaces was investigated by FESEM after gold sputtering and using an accelerating voltage of 2.5 kV. The optical properties of different films were investigated by UV-Vis spectroscopy using a Perkin Elmer Lambda 35 in the range 250-900 nm.

Colour changes of PVA matrix, caused by chitosan and CNC presence at different concentrations, were investigated by means of a spectrophotometer (CM-2300d Konica Minolta, Japan). Data were acquired by using the SCI 10/D65 method whereas CIELAB colour variables, as defined by the Commission Internationale de 1'Éclairage (CIE 1995), were used. Film specimens were placed on a white standard plate and L^*, a^*, and b^*parameters were determined. L^* value ranges from 0 (black) to 100 (white); a^* value ranges from -80 (green) to 100 (red); and b^* value ranges from -80 (blue)

to 70 (yellow). Samples were analyzed in triplicate, and three measurements were taken at random locations on each of the studied films. The total colour difference ΔE^* between PVA and PVA_CH based films and it was calculated as indicated in Eq. 1.

$$\Delta E^* = \sqrt{(\Delta L^*)^2 + (\Delta a^*)^2 + (\Delta b^*)^2} \qquad \text{(Eq. 1)}$$

Gloss value was also evaluated.

Thermal characterization of neat PVA, PVA_CH blend films and PVA_CH_CNC ternary systems was performed by differential scanning calorimetric (DSC) on a TA Instruments DSC Q200 (TA Instruments Inc., USA) under nitrogen atmosphere in the range from -25 to 240 °C at 10 °C min^{-1}, carrying out two heating and one cooling scan. The glass transition temperature (T_g) was investigated during both heating and cooling scan; the melting temperature and enthalpy (T_m and ΔH_m) were determined from the second heating scan, whereas crystallization temperature and enthalpy (T_{cc} and ΔH_{cc}) were determined from the cooling scan. The crystallinity degree was calculated according to the Equation 2:

$$\chi = \frac{1}{(1-m_f)}\left[\frac{\Delta H}{\Delta H_0}\right]*100 \qquad \text{(Eq. 2)}$$

where ΔH is the enthalpy for melting or crystallization; ΔH_0 is enthalpy of melting for a 100% crystalline PVA sample, taken as 161.6 J g^{-1} (Roohani et al., 2008) and (1-m_f) is the weight fraction of PVA in the sample.

PVA, PVA_CH blend films and PVA_CH reinforced films with 3 wt% of cellulose nanocrystals, obtained by acidic hydrolysis of enzymatically pre-treated straw and husk, were subjected to X-ray diffraction analysis. X-ray data were collected with a Philips X'Pert PRO MPD diffractometer operating at 40 kV and 40 mA, with a step size of 0.0167 and 20 s counting time, in the 4-60 ° 2-theta range, using Cu Ka radiation and an X'Celerator detector.

The mechanical behavior of neat PVA, PVA_CH blend films and PVA_CH_CNC ternary films was evaluated by tensile tests, performed on rectangular probes (50 mm x 10 mm) on the basis of UNI

ISO 527 standard with a crosshead speed of 50 mm min^{-1}, a load cell of 500 N and an initial gauge length of 25 mm. The elastic modulus (E), the tensile strength (σ_B) and elongation at break (ε_B) were calculated from the resulting stress-strain curves. The measurements were done at room temperature and at least five samples were tested.

2.6.3. Antibacterial analysis

The antibacterial analysis of PVA_CH based nanocomposite films, reinforced with cellulose nanocrystals extracted from straw and husk by enzymatic pre-treatment and used at the highest content (3 wt%) in the PVA_CH blend, was tested with respect to Xap and Pco bacterial pathogens and both were at a concentration of 1 x 10^6 CFU mL^{-1}. Their subcultures were obtained by bacterial growing for 48-72 h at 25 ± 2 °C using a solid Nutrient Agar (NA) supplemented by Sucrose 5% (NAS). The experiments were carried out using Nutrient Broth (NB) 32% by the liquid medium test (Schaad et al., 1988). Control, PVA, PVA_CH, PVA_CH_3CNC$_{straw_enz}$, PVA_CH_3CNC$_{husk_enz}$ were constituted by 3 replicates each; 5 sterile glass tubes per material, each containing 9 mL of liquid broth (NB) plus 1 mL of Xap or Pco with 1 x 10^7 CFU mL^{-1} to obtain a final bacterial concentration of 1 x 10^6 CFU mL^{-1}, were arranged. In each tube containing the bacterial suspension in NB (except those of Control) , was placed 1 sample (1 cm^2) per nanocomposite films, previously sterilized by C_2H_6O (50%). All tubes were placed on a reciprocal shaker for 48h at 27 ± 2 °C at 150 rpm. Samplings from all tubes were carried out at 1, 3, 12, 24h after bacterial inoculation and serial dilution were carried out and plated on NAS (Nutrient Agar supplemented by 5% of sucrose). After 48h at 27 ± 2 °C the number of Xap and Pco bacterial colonies were counted. All data were statistically elaborated using GraphPad Prism 4 software by analysis of variance (ANOVA) and significance of treatments was determined using Tukey's HSD test ($P \leq 0.05$) (Steel and Jh Dickey, 1997).

2.6.4. Overall migration test, moisture content and food-contact test

The overall migration analysis of neat PVA, PVA_CH blend films and PVA_CH_CNC ternary films was run in triplicate in simulant A (10 (v/v) % ethanol water solution) and simulant D (isooctane) according to Commission Regulation (EU) No 10/2011. Rectangular strips of 10 cm^2 in 10 mL of simulant were used (European, 2011). Samples were maintained at 40 °C for 10 days according to EN-1186 standard (European Standard EN 1186-1: 2002). The simulant was then evaporated and residues weighed with an analytical balance (Sartorius ATILON) with ± 0.01 mg precision. The migration values in mg kg^{-1} of the/each simulant were determined.

The moisture content of the films (MC), equilibrated at 53% RH and 25 °C, was analyzed by drying the samples in a vacuum oven at 40°C for 72 h. Later on, the pre-dried samples were placed in desiccators containing $Mg(NO_3)_2$ until reaching constant weight. Three replicates per film formulation for 1 and 5 weeks were analyzed.

The developed films were putted in contact with sliced prunes and the fungal growth on food samples over the time was observed. Food samples, sterilized by ethanol, were cut and placed on the base of disposable polypropylene Petri dishes. Neat PVA, PVA_CH blend films and PVA_CH_CNC ternary films with a lower thickness around (25±5) μm were produced for this specific characterization in order to guarantee the perfect adhesion of the tested films to the food sample surfaces.

3. Results and Discussion

3.1. Chemical and enzymatic pre-treatments of barley straw and husk

Since the main components of barley fibres are cellulose and, to a lower extent, hemicelluloses, lignin and pectins, the present study proposes two different strategies, one based on a chemical pre-treatment and the second one on a combination of enzymes, both developed to extract and purify cellulose from barley husk and straw. The two approaches were then planned with the aim to remove the largest amount of lignin, hemicellulose and pectin. In fact, the strong interactions of

these compounds with cellulose make the fibres assembled in a very disorganized matrix, in which the components are separated by chemical and/or physical pre-treatments (alkaline and/or concentrated acids, steam explosion) (Wang, et al., 2003; Hendriks and Zeeman, 2009), or, alternatively, by the use of enzymes capable to hydrolyze specific bonds of these bio-polymers (Siqueira et al., 2010). In particular, the recalcitrance of ligno-cellulosic materials is due to lignin, which provides rigidity and integrity to cell wall, pectin, responsible for complexity of these materials, and hemicellulose, which is presents throughout the whole fibre.

We have found that the chemical pre-treatment was effective in increasing the cellulose content in derived materials. In fact, the cellulose increased from 56.2 and 45.7% to 75.2 and 62.8% in chemically pre-treated straw and husk matrices, respectively (Table 1). Therefore, on the basis of these results, it was estimated that chemical pre-treatments permitted to achieve a cellulose purification fold for straw and husk (calculated as the ratio between the cellulose content found in the purified matrix and that in raw starting material) of 1.34 and 1.29 (Table 1), respectively.

In the enzymatic pre-treatment, prior to submit straw and husk to enzymes digestions, the raw materials were washed with distilled water in order to remove the more hydrophilic interfering substances. Afterwards, the matrices were repeatedly treated with alkali to detach and solubilize lignin and the alkaline soluble pectins from the fibres. The solid residue was then autoclaved in order to break down the composite ligno-cellulosic residues, by combining the effects of temperature and pressure (120 °C and 1.5 atm). Autoclaving is considered a useful step to break down fibres and improve the accessibility of the hydrolytic enzymes to cellulose. In fact, the following step was the incubation of the solid residues with Pectinase. This class of enzymes, widely studied for its ability to degrade cell wall and its involvement in phytopathogenic processes, has attracted noticeable attention for their use in enzymatic procedures aimed at purifying cellulose from ligno-cellulosic materials. The commercial formulation of Pectinase chosen for our experiments provides some hydrolytic activities, which show a high degree of substrate specificity: pectin lyase (hydrolysis of 4,5-unsaturated oligogalactouranotes by ß-elimination),

polygalacturonase (hydrolysis of pectin polymers into galacturonic acid), and pectin methylesterase (hydrolysis of methyl esters of homogalacturonan). Cellulase, the other commercial enzyme formulation employed in our experiments, was chosen for its capacity to randomly break down the non-crystalline parts of cellulose, by hydrolyzing theendo-1,4-β-D-glycosidic linkage sand cellooligosaccharides.

The enzymatic cellulose pre-treatments permitted to increase the content of cellulose in straw and husk derived matrices from 56.2 and 45.7 (starting raw materials) to 72.6 and 81.0% (Table 1), respectively. On the basis of these data, the enzymatic pre-treatments permitted to achieve for straw and husk a cellulose purification fold of 1.29 and 1.77 (Table 1), respectively. The latter result indicates as the enzymatic pre-treatments of husk was the most effective in increasing the percentage content of cellulose in the derived matrices.

Morphological analysis was performed with the aim of examining the structure of barley straw and husk, before and after chemical and enzymatic pre-treatments. FESEM images of pristine fibres from barley straw are reported in Figure 1a,while the images of the same fibres after chemical and enzymatic pre-treatments are reported in Figure 1b and Figure 1c, respectively. The surface of pristine barley straw consists of many cylindrical wax rods, arranged at different angles, as previous observed by others authors (Amer et al., 2007; Wiśniewska et al., 2003). Cross section of barley straw (inset) showed hollow tubules and various cell types of the straw wall can be seen, including parenchyma cells and vascular bundles (Kristensen et al., 2008). It was demonstrated that the morphology and composition of plant waxes changes with plant development and, that the chemical composition of the wax determines the shape and size of the crystals (Wiśniewska et. al., 2003). The most apparent effect of the chemical pre-treatment is the partial defibrillation, or separation of individual fibres and cell types of barley straw. Although the pre-treated material is quite heterogeneous and contains larger pieces that are easily recognised as straw, a significant fraction consists of cells that are either completely or partially separated from each other (Figure 1b) (Luzi et al., 2014). In the case of enzymatically pre-treated fibres, the defibrillation process seems to be

more efficient and some spirals, recognizable as vascular protoxylem structures, appeared. They were visible as a consequence of a more effective removal of hemicellulose and lignin components (Figure 1c).

FESEM images of the surface and cross section of the pristine fibres from barley husk are reported in Figure 1d, whereas in Figure 1e and Figure 1f the images of the same fibres are reported after chemical and enzymatic pre-treatments, respectively. The surface of pristine husk fiber was found to be smooth, with cellular units filled by lignin and fatty substances (El Halal et al., 2015) (Figure 1d), with regular protuberances, longitudinally elongated epidermal cells having thick walls visible. The surface of untreated barley husk was rigid and some phytoliths were visible, which were decay-resistant silica bodies that protect the fibres against biodegradation (Kim et al., 2008). As visible in the inset, the bast layer below the outer epidermis was made up of more or less thickened sclerenchyma fibres, thin-walled parenchyma and vascular bundles (Briggs, 2012). Figure 1e shows that chemically pre-treated barley husk consisted of separated and modified fibres, peeled off from the initial connected structure and fully exposed. This treatment mainly removed lignin and caused some physical changes such as loosening of the matrix, partial degradation of hemicellulose, dismantling of vascular bundles. In addition, this treatment acted as a swelling agent in improving the accessibility of cellulose to the following chemical actions (Chandel et al., 2013). These fibres, if compared to those chemically pre-treated obtained from barley straw (Figure 1b), appear less individualized and the elementary filaments show a more compact structure (even if the spongy parenchyma structure seems to become more visible). This indicates that the chemical pre-treatment could be less effective in disentangling the fibres, but certainly more efficient in removing adhesive substances and non-cellulosic components from the fibre surface.

In the case of enzymatic pre-treated fibres obtained from barley husk (Figure 1f), the refining of fibres (less rough surface) determined by the pectinase/cellulase treatments was accomplished by a selective removing of waxy epidermal tissue, adhesive pectins, hemicellulose that appears as debris and non-cellulosic components (Ouajai and Shanks, 2005; Pakarinen et al., 2012).

FTIR spectra of pristine barley straw, chemically and enzymatically pre-treated fibres and nanocrystals extracted from the two pre-treated materials are shown in Figure S1 a,b). Characteristic signals of pristine barley straw were detected at 3420, 2923 and 2852 cm^{-1} and related, respectively, to the stretching vibrations of OH and CH bonds. The peak at 1737 cm^{-1} in pristine barley straw could be both attributed to ester, acetyl and uronic groups of hemicellulose, and ester bond of the carboxyl groups of ferulic acid and p-coumaric characteristic of lignin component (Li et al., 2012). This peak completely disappeared in the pre-treated fibres, due to the removal of hemicellulose and lignin from the straw, as a result of the chemical treatment. The band at 1640 cm^{-1}, visible even in the signal of chemically pre-treated barley straw, was due to the bending of absorbed water (Sun et al., 2002). The absorption band of the lignin at 1508 cm^{-1} was visible only in the signals of raw materials, whereas the absence of this peak in the signals of chemically and enzymatically pre-treated fibres confirms their efficacy in the removing of lignin. Also the peaks detected at 1462 and 1429 cm^{-1} could be attributed to lignin, and they respectively represent the in plane deformation of aromatic ring C-H and the C = C stretching of aromatic rings (Jacobsen and Wyman, 2002; Sun et al., 2005). The peak at 1235 cm^{-1} in the pristine barley straw, attributable to the C=O stretching of hemicellulose, disappeared in the spectrum of the chemically pre-treated straw. The bands at 1383, 1317, 1162 and 897 cm^{-1} were typical of cellulose and are related, respectively, to C-O stretching, CH_2 wagging, C-O-C asymmetric stretching and C-O-C stretching of β-1,4-glycoside bond (Mood et al., 2013). These peaks, related to the cellulosic fraction, are all more visible both in the chemically and enzymatically pre-treated straw (Sun et al., 2005). FTIR spectra of pristine barley husk, chemically and enzymatically pre-treated fibres and nanocrystals extracted from the two pre-treated materials were reported in Figure S1 c,d). The peak at 3450 cm^{-1} in the spectrum of pristine barley husk was due to stretching of the OH bond. This peak shifts to 3490 cm^{-1}, 3430 cm^{-1}, 3420 cm^{-1} and 3444 cm^{-1}, respectively for chemically pre-treated fibres and enzymatically pre-treated fibres, CNC from chemically and enzymatically pre-treated fibres. The peaks at 2923 and 2852 cm^{-1} were due to the asymmetric and symmetric

441 stretching of the CH bonds in cellulose and hemicellulose components. The weak signal at 2115 cm^{-1}
442 could be attributable to the S-H stretching (due to the presence of silica), that disappeared in the
443 spectra of the CNC obtained from the two pre-treated fibres, whereas it was still visible both in the
444 chemically and enzymatically pre-treated materials (Bledzki rt al., 2010). A peak attributed to C=O
445 stretching of acetyl ester and uronic groups of hemicellulose (and ester bond of ferulic and p-
446 cumaric groups in lignin) was visible at 1726 cm^{-1}. The peak at 1635-1640 cm^{-1} was associated to
447 the stretching and bending of OH water bond, the peaks at 1155 and 1036 cm^{-1} were associated with
448 the fraction of carbohydrates, whereas C-C and C-O stretching and C-O-H bending signals can be
449 found between 1400 and 1200 cm^{-1}. In particular, the peak at 1035 cm^{-1} was due to
450 hemicellulose/cellulose C-O stretching and aril-OH of lignin. At 1466 cm^{-1}, the asymmetrical
451 bending of CH_3 and (-OCH_3) and 1513 cm^{-1} (stretching aromatic C=C) present in lignin can be
452 found (Ang et al., 2012). The signal at 1256 cm^{-1} was due to the structural cellulosic component,
453 whereas the one at 1398 cm^{-1} was due to the presence of phenolic compounds (C = C stretching of
454 the aromatic ring and phenolic OH bending (1410-1310 cm^{-1}) (Cozzolino et al., 2015).
455 Results from thermogravimetric analysis (derivative curves) for pristine and pre-treated fibres were
456 reported in Figure 2 a,b) and Figure 2 c,d), respectively for chemically and enzymatically pretreated
457 barley straw and husk. Three major areas of weight loss can be detected on DTG curves, the first
458 peak is due to the dehydration of the straw fiber (or husk), while two other peaks between 200 and
459 400 °C on the DTG curves are detected: the first peak at 288 °C is due to the decomposition of the
460 fibres by depolymerization of hemicelluloses and pectins, followed by a second peak at 330 °C,
461 which reflects the degradation of the cellulose (Bouasker et al., 2014; Palumbo et al., 2015). The
462 peak at 400 °C is due to the decomposition of lignin. The absence of the shoulder observed at lower
463 temperatures (under 300 °C) confirms the elimination of hemicellulose in chemically and
464 enzymatically pre-treated straw (Abraham et al., 2015; Singh et al., 2015). The peak temperatures at
465 the maximum of degradation rate are different for the two different treatments (332 °C for barley
466 straw fibres after chemical pre-treatment and 340 °C after enzymatic pre-treatment): this result

467 indicated a moderate increase in the thermal stability of enzymatically pre- treated fibres, due to
468 both better removal of non-cellulosic material present in the fibre (confirmed by a lower value of
469 residual mass at the end of the test for enzymatic pre-treated straw with respect of chemically
470 treated fibres and already evidenced by FESEM investigation) and presence of high crystalline
471 cellulosic components. In the case of barley husk, we observed higher residual mass at the end of
472 the test for untreated husk (28.6%) with respect of untreated straw (23.6 %), due to the presence of
473 ash (silica based), whereas no differences could be found for the two different treatment in terms of
474 residual mass. TG curves revealed, also in this case, a peak between 40°C and 130°C, which
475 corresponds to the vaporization of water and two decomposition steps, more likely attributable to
476 thermal decomposition of the hemicellulose and the glycosidic linkage of the cellulose (Mamun and
477 Bledzki, 2014). The peak at 350–390°C is due to α –cellulose decomposition, whereas the signal
478 due to lignin (190–500°C) is slightly broader with a maximum value (peak) at about 350°C. Among
479 the three major components, the hemicellulose is the easiest to decompose due to branched
480 structural features with short side chains: its peak completely disappeared in the case of enzymatic
481 pre-treated husk and a sharp peak at $T_{max,}$ due to highly specific and highly ordered structure of
482 cellulose obtained in the case of enzymatic pre-treatment was detected. However, in the case of
483 chemically pre-treated fibres, a weak shoulder and a less intense peak related to cellulose
484 devolatilization are visible in the DTG profile, indicating a less ordered structure for cellulosic
485 component and limited effect of the treatment in the removal of no cellulosic material (Raj et al.,
486 2015).
487
488 **3.2. Cellulose nanocrystals from barley straw and husk**
489 The micro-fibres obtained after both the chemical and enzymatic pre-treatment of barley straw and
490 husk were hydrolyzed by acid in order to isolate cellulose nanocrystals (CNC) to be used as
491 reinforcement phases in the selected polymer matrices. Cellulose nanocrystal suspensions were
492 prepared by applying the same procedure to the two typologies of barley wastes. The highest yield

493 of reaction (around 12%) was measured for enzymatically pre-treated husk. Lower values of yield
494 were registered for chemically treated husk (CNC_{husk_chem} – ca. 4%) and pre-treated straw
495 (CNC_{straw_enz}, and CNC_{straw_chem}– about 5%). The obtained low hydrolysis yields were related to
496 both raw material source (straw or husk) and procedures applied (chemical or enzymatic pre-
497 treatment), meaning that some optimizations of the procedures might be required for these specific
498 materials. However, in this first approach, we preferred to set the same extraction procedure (in
499 terms of CNC production) for all the precursors in order to establish the best typologies of barley
500 residue to be used for CNC synthesis, applying well known and previous published hydrolysis
501 receipts (Fortunati et al., 2012; Fortunati et al., 2014; Fortunati et al., 2015; Fortunati et al., 2013).
502 Figure 3 shows the morphological investigation of CNC obtained after hydrolysis procedures (45
503 °C, 30 min) from different barley material. Almost all the extracted nanostructures showed the
504 typical needle-like structure of CNC. FESEM images show that most cellulose nanocrystals
505 obtained from the hydrolysis of both chemically and enzymatically pre-treated barley fibres were
506 characterized by an acicular structure, typical of cellulose nanocrystals or whiskers; however, some
507 differences in the shape and dimensions (the average dimensions of CNC were obtained after the
508 analysis with ImageJ software of FESEM micrographs) of CNC extracted from straw and husk
509 occurred. In particular, a more spherical shape with the presence of some none-perfectly reacted
510 material and residues, characterized by different shape and aggregation levels, were revealed for
511 CNC_{straw_chem}. The obtained shape and dimensions for these CNC_{straw_chem} was different from the
512 typical acicular structure of CNC extracted with the same procedure from other similar plant
513 residues (Fortunati et al., 2014; Fortunati et al., 2015; Fortunati et al., 2013), and the possible
514 presence of residual sugars, or even hemicellulose in the sample, underlined the non-perfect
515 efficacy of the applied hydrolysis receipt for this precursor, confirmed by a low reaction yield
516 (around 5%). Differently, although some spherical residues were present and some unreacted
517 material visible, FESEM image for CNC_{straw_enz} showed nanocrystals with the typical acicular
518 structure and with dimensions around (270±40) nm in length and (15±5) nm in width, as recently

519 reported for barley residues (Espino et al., 2014). However, the presence of residues justify the low
520 reaction yield (around 4%) obtained for this barley material. A different behavior was observed for
521 CNC extracted from husk, both by chemical and enzymatic pre-treatment. In fact, both the
522 CNC_{husk_enz} and CNC_{husk_chem} showed the typical acicular structure, with no residues or unreacted
523 material visible by FESEM, underlining the effectiveness of the applied hydrolysis receipt for husk.
524 Moreover, also in this case, it is clearly visible that the best performance of the hydrolysis was
525 obtained after the enzymatic pre-treatment of the fibres. In particular, the CNC_{husk_enz} showed the
526 typical dimension ranging from 150-250 nm in length and of about 10 nm diameter (Fortunati et al.,
527 2014; Fortunati et al., 2015; Fortunati et al., 2013). Finally, nanocrystals of (280±70) nm in length
528 and with a higher diameter (30±10) nm were obtained from chemically pre-treated husk
529 (CNC_{husk_chem}).
530 The different effects of the applied treatments on barley straw and husk were also highlighted by X-
531 ray diffraction results shown in Figure S2 a. The extracted CNC show the diffraction features
532 typical of cellulose I crystal domains. In the native state, the cellulose shows a semicrystalline
533 structure with crystalline domains of cellulose I with parallel chains connected side-by-side via
534 hydrogen bonding in flat sheets embedded in an amorphous phase made by lignin and
535 hemicellulose. Regeneration and mercerization of cellulose based materials induce a transformation
536 from cellulose I structure to cellulose II, where the chains are stacked to form corrugated sheets
537 bounded together by a hydrogen bonding network. All XRD patterns for different CNC showed the
538 main peak at 22.7° (a low shift was detected only for CNC_{straw_chem}), that is indicative of the
539 distance between hydrogen bonded sheets in cellulose I domains. The other three peaks,
540 corresponding to the doublet peaks at 14.8° and 16.6°-16.8°assigned to (1-10) and (110) lattice
541 plane and the peak at 34.5°-34.7°, are also typical of cellulose I, which arises from ordering along
542 the fibre direction and it is sensitive to the alignment of chains into the fibrils (Besbes et al., 2011).
543 All the others peaks depicted in Figure S2 a are typical of cellulose II. The lowest intensity of both
544 the main peak (at 22.7° cellulose I) and peaks around 15-16° was registered for CNC_{husk_chem} and

545 CNC_{straw_enz}, whereas an intense main peak (22.7° cellulose I) was registered for CNC_{husk_enz},
546 underlining again the effectiveness of the enzymatic pre-treatment, especially for barley husk, in the
547 extraction of cellulose nanostructures and confirming the FESEM results (Figure 3 d) and the
548 reaction yield values.
549 In the aim of using the extracted CNC as reinforcement phases in polymeric based formulations, the
550 thermal stability has to be ensured. Thermogravimetric analysis was performed and the results of
551 thermal degradation of CNC structures in terms of derivative curves of the weight loss are reported
552 in Figure S2 b. All the thermograms showed a multi-step degradation with three weight loss events
553 (Espino et al., 2014). The water evaporation, due to the humidity absorbed on the CNC surfaces,
554 occurred, for all the studied nanostructures tested in their dried form, between 30 and 100 °C with a
555 mass loss lower than 10%. During the degradation of the cellulose (second and third peaks)
556 depolymerisation, dehydration and decomposition of glycosidic units occurs (Roman and Winter,
557 2004). Two relevant peaks due to cellulose degradation can be observed in CNC DTG curve: the
558 first (T_1) at 280-290 °C and the second around 350 °C. Since sulfate groups by bonding to the
559 glucose units decrease the thermal stability of the CNC (Roman and Winter, 2004), the first peak
560 can be related to the CNC-SO_4^{2-} and the second one (main peak - T_{max}) to CNC-OH. Regarding the
561 T_{max} of CNC-OH degradation, a higher stability of CNC isolated from barley husk, especially in the
562 case of an enzymatic pre-treatment of the waste (T_{max}=356 °C), was measured, confirming previous
563 results. High stability (T_{max}=352 °C) was also registered for CNC_{straw_enz}. Moreover, CNC extracted
564 from barley husk showed the most intense peaks (both the peak around 290 °C and the main peak
565 around 350 °C), highlighting a well-defined structure of both cellulose II and cellulose I. Finally,
566 lower values of residual mass calculated at 900 °C were registered for CNC_{husk_enz} (15%) with
567 respect to the others CNC (18%, 26% and 28% for CNC_{husk_chem}, CNC_{straw_enz}, and CNC_{straw_chem},
568 respectively), confirming previous results and discussion.
569 Analysis of FTIR spectra for CNC confirmed that the peaks related to the cellulosic fraction,
570 detected in the signals of pre-treated fibres, become more evident in the case of cellulose

571 nanocrystals extracted from the same source (Sun et al., 2005). In particular, the peak found at 897
572 cm^{-1} for the pristine barley straw, that shifted to 894 cm^{-1} and 893 cm^{-1}, respectively for chemically
573 and enzymatically pre-treated fibres, moves to 894 cm^{-1} and 864 cm^{-1} in the case of nanocrystals.
574 The sharp and intense peak at 1079 cm^{-1} visible in the signal of pristine barley straw, attributed to
575 the C-O stretching, shifted to 1059 cm^{-1} for chemically pre-treated fibres and 1058 cm^{-1} for
576 enzymatically pre-treated fibres, can be measured in the case of CNC, at 1060 cm^{-1} for CNC
577 extracted from chemically pre-treated straw and 1061 cm^{-1} in the case of CNC from enzymatically
578 pre-treated straw (Azizul et al., 2012). In the case of barley husk, the signal at 1050 cm^{-1} can be
579 assigned to the deformation of C-O bond in the aliphatic esters. This signal, shifted to 1057 cm^{-1} in
580 chemically pre-treated fibres and 1055 cm^{-1} in enzymatically pre-treated fibres, moves to 1060 cm^{-1}
581 and 1059 cm^{-1}, respectively for CNC extracted from chemically pre-treated and enzymatically pre-
582 treated fibres. The peak at 900 cm^{-1} is indicative of the frequency group of C1 ring, characteristic of
583 the β-glycosidic bonds traceable in sugar units (Bledzki et al., 2010). As in the case of barley straw,
584 the signals attributable to the cellulosic fraction, present both in pretreated barley husk and
585 corresponding CNC, became more evident, whereas the one related to hemicellulose and lignin
586 fractions disappeared (1730, 1513 and 1466 cm^{-1}).
587
588 **3.3. PVA_CH nanocomposite characterization**
589 ***3.3.1. Morphological analysis, transparency and colorimetric analyses***
590 The microstructure of the cross-section surfaces of neat PVA and PVA_CH based nanocomposites
591 reinforced with different content and typologies of cellulose nanocrystals were investigated by
592 means of FESEM (Figure 4 Panel A), with the purpose of evaluate the effect of chitosan and CNC
593 presence on the morphological behavior of PVA based system. PVA film fractured surface appeared
594 smooth, uniform and homogeneous (Kavoosi et al., 2014) (Figure 4 Panel A, a)) typical of a
595 semicrystalline polymer (Fortunati et al., 2016), highlighting the excellent film-forming properties
596 of PVA in solvent casting process, in agreement with other authors (Fortunati et al., 2016; Fortunati

et al., 2013). PVA_CH film (Figure 4 Panel A, b)) showed uniform and homogeneous surface without evidencing phase separation, irregularities, pores, cracks, droplets or air bubbles (Bonilla et al., 2014). This result underlines the high compatibility of the two polymers (Bonilla et al., 2014; Tripathi et al., 2009). However, the presence of chitosan in PVA film slightly increased the roughness of cross section surface respect to neat PVA, due to the brightness nature of chitosan matrix (Figueiredo et al., 2015). The aspect of the PVA_CH_CNC nanocomposites was wavy respect to PVA_CH film due to the interactions between the filler and the polymer blend (Roohani et al., 2008). The fractured surfaces of PVA_CH based nanocomposites appeared homogenous without any phase separation, and no large aggregates due to the presence of CNC were detected on the film surfaces. Moreover, no particular alteration were induced by the presence of CNC also in the case of 3 wt% CNC based systems.

Transparency and colour of a package material are important parameters to be considered. In fact, the final external quality of the packaging influences consumer acceptance and commercial success of the different products. Transparency properties of PVA and PVA_CH based nanocomposites were characterized by UV-Vis spectrophotometry (Figure 4 Panel B a,b). Figure 4 Panel B,a shows the UV-Vis spectra of PVA and PVA_CH based systems reinforced with 1 wt% CNC extracted from straw and husk by chemical and enzymatic pre-treatments (CNC_{straw_chem}, CNC_{husk_chem}, CNC_{straw_enz} and CNC_{husk_enz}), whereas Figure 4 Panel B a shows the UV-Vis spectra of PVA and PVA_CH nanocomposites reinforced with 1 wt% and 3 wt% of CNC_{straw_enz} and CNC_{husk_enz}. UV-Vis analysis confirmed that PVA is a transparent polymer (transmittance of 94.2% at a visible wavelength of 600 nm): the transparency values at the same wavelength for PVA_CH system was the sam, but decreases progressively reducing the wavelength (in the range 250-450 nm). PVA_CH films showed an absorption band centered at 280 nm caused by the presence of chitosan in PVA_CH film and due to the presence of double bonds, particularly those of C–O (Abdelrazek et al., 2010; Bonilla et al., 2014). On the contrary, the transparency of PVA_CH nanocomposites was not affected, in the range of 450-900 nm, by the addition of CNC, whereas a light barrier between

250-450 nm was found. In fact, the presence of CNC in PVA_CH based systems reduced the transmission capability at the wavelengths ranging from 300 to 450 nm. This effect was caused by the fraction of the CNC, which can exert a significant influence on the UV transmittance (Figure 4 Panel B, b) (Fortunati et al., 2013). In any case, all the produced nanocomposite films maintained good levels of transparency, also in the case of the highest content of cellulose, due to the absence of aggregates and homogeneity of the PVA_CH_CNC films, confirming what already observed by FESEM analysis (Figure 4 Panel A).

The colorimetric and gloss analysis of PVA and PVA_CH based films was performed to evaluate the influence of the chitosan and CNC on the PVA optical properties. Some differences in the CIELab coordinates (L^*, a^*, b^*) and ΔE^* between PVA_CH based nanocomposites were observed (Table 2). These differences were induced by the intrinsic colour of the components (chitosan powder and CNC water suspension) used to realize the different nanocomposite films. High lightness values were observed for PVA (L^* = 99.10±0.04) and for PVA_CH based films and no particular variations were observed for the different nanocomposite formulations. However, lower value of L^* was registered for PVA_CH_3CNC$_{straw_enz}$ (L^* = 96.91 ±0.28), and this could be due to the decrease of lightness value attributed to the high content of CNC into the polymeric blend. Negative and low values were obtained for the a* coordinate but no particular differences were observed among the different formulations. Moreover, the lowest value was obtained for PVA_CH film (-0.22±0.03); this effect could be related to the presence of chitosan in PVA matrix. By adding different contents of CNC, the values attributed to the a*coordinate increase.

Positive values were obtained for b* coordinate, indicating a deviation towards a yellowish colour; this result was in agreement with UV-Vis analysis (Figure 4 Panel B a,b), in fact the transparency of different formulations decreased in the range of wavelength centered around 250-450 nm. Moreover, the highest values of b* coordinate were registered for PVA_CH_3CNC$_{straw_enz}$. This result highlighted that the increment of CNC content led to an evident shift to yellow colour with respect to the film reinforced with 1 wt% of CNC$_{straw_enz}$ (Table 2). However, the decrease of L*

values, combined with the increase of b* data, indicated that a yellowish colour appeared in the film. The reduction of lightness was considered helpful to prevent oxidative deterioration in packaged foodstuffs (Wang et al., 2012). The colour differences ΔE^* were estimated between the PVA and PVA_CH based films. The highest ΔE^* values between the PVA and nanocomposite films was approximately close to 5, recorded for PVA_CH_3CNC$_{straw_enz}$.

The gloss (Table 2) of PVA and PVA_CH based systems was influenced by the presence of cellulose nanocrystals (Luzi et al., 2016). The gloss values decreased as a function of the filler percentage, however the higher reduction was around 11° and was registered for PVA_CH_3CNC$_{husk_enz}$ (225 ± 2) ° respect to PVA film (236 ±4) °. The high gloss values could be related to the good distribution of chitosan into PVA matrix, indicating the high compatibility of the two polymers (Bonilla et al., 2014; Tripathi et al., 2009) and the good distribution of CNC into polymeric blend, as previously observed and confirmed by FESEM investigations (Figure 4 Panel A).

3.3.2. Thermal, X-ray and mechanical characterizations

The effects of both chitosan and extracted CNC from straw and husk residues on the thermal properties of the PVA matrix were investigated by DSC measurements and the properties of films obtained by analysis of cooling and second heating scans are summarized in Table 3. During the cooling scan, slight increases (about 3 °C) were observed in the glass transition temperature (T_g), which were induced by the presence of CH and, a shift of about 5 °C was detected for the systems reinforced with different typologies and contents of CNC. This effect induced by both the CH and CNC presence was also measured during the heating scan and it can be explained by considering the presence of interactions through hydrogen bond formation, which implies an effective increase of T_g values. Moreover, a clear decrease in the enthalpies related to the crystallization phenomena was detected during the cooling induced by the addition of CH in PVA matrix, as previously reported (Bonilla et al., 2014), moreover a decrease of the crystallization temperature (T_c), that

675 presented a shift of about 15 °C for PVA_CH respect to the PVA neat film (PVA: T_c=191.3±0.8 °C
676 and PVA_CH: T_c=177.5±0.8 °C), was observed. The presence of CNC did not particularly affect
677 the thermal response of PVA_CH blend both during the cooling and the second heating scan; a
678 slight increase in the crystallization enthalpies and temperatures was registered for the formulations
679 reinforced with CNC extracted by an enzymatic pre-treatment (T_c around 180°C), suggesting the
680 potentiality of this sustainable pre-treatment in obtaining cellulosic materials with higher propensity
681 to induce nucleation. This effect was then confirmed also in the PVA_CH based formulations
682 loaded with 3 wt% of CNC_{straw_enz} and CNC_{husk_enz} although their effect was not so evident as
683 expected. The nucleation effect, typical of CNC, previously reported for different polymer matrix
684 and also for neat PVA based formulation loaded with this nano-reinforcements (Fortunati et al.,
685 2012; Fortunati et al., 2013), was not so evident here, since the presence of chitosan was
686 predominant in the thermal response of produced PVA_CH based formulations. Finally, no
687 particular variations were found in the case of *X* (%), measured both during the cooling and heating
688 scans.
689 In order to better investigate the effect of chitosan and CNC presence in the produced blends, XRD
690 analysis of PVA and PVA_CH based formulations was performed (Figure 5a). The X-ray
691 diffraction profile of neat PVA film shows an intense reflection peak at 2θ = 19.7˚ and a shoulder at
692 2θ = 17.61°, typical of the crystalline atactic PVA (Ricciardi et al., 2004), that can be assigned to a
693 mixture of (101) and (10Í) reflections. Another peak located at 41.3° also confirms the
694 semicrystalline nature of PVA (Hemalatha et al., 2014). Moreover, several less intense crystalline
695 peaks at 2θ = 12.0, 14.70, and 29.82 degrees were detected, that can be assigned to a mixture of
696 (110), (101), (10ī), (200), (201) and (20ī) (Lee et al., 1996). In the case of PVA_CH blend, the film
697 showed the typical fingerprints of semicrystalline chitosan visible at 2θ = 13.35° and 19.88°
698 (superimposed with the signal of PVA), related to crystal I and crystal II in chitosan structure,
699 comparable with that observed in the diffractogram reported by Rinaudo et al. (Rinaudo, 2006). The
700 reduced intensity for this last peak confirmed that the semicrystalline structure of PVA was

decreased upon blending with chitosan (as already observed in DSC characterization). When 3 wt % of CNC_{straw_enz} and 3 wt% of CNC_{husk_enz} were incorporated in the films, the XRD profiles exhibited the characteristic peaks of both CNC and PVA_CH blend, basically the diffractogram showed peaks already observed in Figure S2 a (typical peaks of cellulose-I structure) around 2θ = 34.7°, assigned to (004) plane, with higher intensity both in PVA_CH_3 CNC_{straw_enz} andPVA_CH_3 CNC_{husk_enz}. The peak located at 19.6°, plane (200), had a reduced intensity, whereas increased value can be seen in the case of the peak located at 13.53°, confirming the predominant effect of chitosan in overall crystallinity of produced films.

Films for food packaging are required to maintain their integrity during the use (Kanatt et al., 2012) and, according to this, tensile tests were performed for PVA matrix and PVA_CH blend based formulations, with the aim of investigating the effects of both chitosan and extracted CNC from straw and husk residues on the mechanical response of produced films. These results are summarized in Table 4, while typical stress-strain curves for neat PVA, PVA_CH blend and PVA_CH based formulations are shown in Figure 5b, The addition of 10 wt % of chitosan to PVA matrix provoked a reduction in the mechanical response of the system, with a decrease of both tensile strength and elongation at break values for PVA_CH blend respect to neat PVA film (Bahrami et al., 2003; Bonilla, Fortunati et al., 2014).

On the other hand, CNC at 1 wt% into PVA_CH blend, were able to increase the elongation at break values: this result is more evident for PVA_CH_1CNC_{straw_enz} and PVA_CH_1CNC_{husk_chem} films, that showed also an increase in the Young's modulus and tensile strength. The interaction between polymers and CNC resulted in an efficient load transfer between nanofillers and polymer chains, especially in the case of films containing CNC_{straw_enz} and CNC_{husk_chem} at 1 wt%, which makes the nanocomposites stronger but maintains, at the same time, the deformation behavior of neat PVA (ε_B about 200%). This result can be certainly correlated to CNC morphological aspect previously discussed in paragraph 3.2, that evidenced the presence of some none-perfectly reacted material and residues in the case of CNC_{straw_chem}, justifying the low deformability registered for this

727 specific system. On the other hand, the typical acicular structure of CNC, revealed as completely
728 free of defects for CNC_{husk_chem} and CNC_{husk_enz} and weakly compromised in the case of
729 CNC_{straw_enz}, is responsible for the good mechanical response of films containing these nanofillers.
730 The promising results of tensile characterization obtained for PVA_CH films in the case of CNC
731 extracted from straw and husk after the enzymatic pre-treatment induced us to consider the
732 possibility of increasing their mechanical performance by adding higher amounts of nanofillers (3
733 wt% of CNC_{husk_enz} and CNC_{straw_enz}).
734 Actually, this effect of cellulose nanocrystals was confirmed and enhanced when 3 wt% were
735 added. In this case, an increase of Young's modulus and tensile strength respect to both PVA neat
736 film and PVA_CH blend was registered for ternary formulations, whereas the stretchability was
737 increased with respect to PVA_CH blend and maintained at the level of PVA matrix. In conclusion,
738 the results of mechanical characterization underlined that, even if the presence of the chitosan,
739 selected for its antimicrobial properties, can negatively compromise the mechanical response of
740 PVA in terms of deformability, the addition of a very low content of a bio-based/natural nanofiller
741 as CNC to the selected polymer matrices can positively counterbalance and modulate the final
742 mechanical response of PVA_CH blend, with a right compromise between elastic and plastic
743 response of the film, useful for the final practical application.
744
745 ***3.3.3. Antibacterial properties***
746 The antibacterial test of PVA_CH based nanocomposites, reinforced with CNC extracted from
747 straw and husk by enzymatic pre-treatment and used at the highest content (3 wt%) in the PVA_CH
748 blend, was tested with respect to Xap and Pco bacterial pathogens. Xap growth pointed out its
749 capacity to increase exponentially its population in control as well as in association with PVA and
750 PVA_CH films (Figure 6 a). Instead, in PVA_CH_3CNC_{straw_enz} and PVA_CH_3CNC_{husk_enz} films,
751 the bacterial growth was particularly reduced and this effect was more evident with
752 PVA_CH_3CNC_{straw_enz} film for which Xap growth, after 24 h from its inoculation, showed values

753 proximal to the initial one (3.6 x 10^6 CFU mL^{-1}) (Figure 6 a). Concerning Pco development, respect
754 to different films placed simultaneously in different formulations, the best results were recorded
755 after 3 h by PVA_CH_3CNC$_{straw_enz}$ and PVA_CH_3CNC$_{husk_enz}$ films, with bacterial values of 7.6 x
756 10^5 CFU mL^{-1} and of 6.5 x 10^5 CFU mL^{-1}, respectively (Figure 6 b). After 24 h, the highest
757 bacterial values were recorded for PVA films (1.7 x 10^8 CFU mL^{-1}), whereas the Pco values with
758 PVA_CH_3CNC$_{straw_enz}$ and PVA_CH_3CNC$_{husk_enz}$ films, were of 6.9 x 10^7 CFU mL^{-1} and of 6 x
759 10^7 CFU mL^{-1}, respectively (Figure 6 b). The phytobacteria considered in the present study resulted
760 particularly significant to evaluate the potential antimicrobial activity of different nanocomposites
761 as active packaging films developed. The Xap quarantine bacterial pathogen, resulted successfully
762 inhibited in its development especially by using the PVA_CH_3CNC$_{husk_enz}$ film. The performance
763 obtained by these nanocomposite films resulted particularly relevant taking into account that this
764 bacterium it is able to survive, until 5 months, in ice-box conditions of -2°C to +2°C, even lower
765 than those make good use at an industrial level as, for example, for the fresh fruit packaging
766 (Bulletin OEPP/EPPO, 2006). The Pco bacterial strain is able to cause severe soft rot during storage
767 on a wide range of vegetables and fruits (Toth et al., 2003). By present study Pco growth inhibition
768 resulted reduced by the presence of PVA_CH_3CNC$_{husk_enz}$ film, although a less relevant effect over
769 time was registered for Pco pathogen respect to Xap.
770
771 ***3.3.4. Validation of the practical use of the proposed formulation at an industrial level: overall***
772 ***migration test, moisture content and food-contact test***
773 PVA_CH based formulations could find different final applications at a practical level as, for
774 example, biodegradable supports in biomedicine and tissue engineering, as coating materials and/or
775 also as novel packaging formulations. In the present work, we have focused on this third possible
776 solution and some specific characterizations were performed in order to validate the practical use of
777 the proposed systems at industrial level.

778 Overall migration test with food simulants results are shown in Figure 7. The test permits to
779 simulate and demonstrate, by using two different simulants, ethanol 10 (v/v)% and isooctane (A and
780 substitutive D2, respectively), the behavior of potential food packaging in contact with the
781 foodstuff. The overall migration levels using both food simulants for all the studied PVA and
782 PVA_CH based systems were below the migration permitted limits, taking into consideration that
783 the current European legislation establishes that the material migrated need to be lower of 60 mg kg^{-1}
784 simulant (European Commission Regulation EU 10/2011). The maximum migration level (3.3 mg
785 kg^{-1} simulant) was detected for PVA_CH_3CNC_{straw_enz} after 10 days in ethanol. The high values of
786 PVA based systems in contact with simulant A were due to the hydrophilic nature of polymer
787 matrix selected for this research, that showed an high affinity with polar solvent as water solution
788 (Fortunati et al., 2013).
789 The analysis of the total migration values in isooctane after 2 days at 20 °C revealed that the
790 maximum migration level was detected for PVA_CH_1CNC_{husk_chem}, with the value of 0.09 mg kg^{-1}
791 simulant. However, all the migration values of PVA are well below the overall migration legislative
792 limits, confirming the possibile use of proposed formulations for food-packaging.
793 Table 5 shows the moisture content (MC) of PVA and PVA _CH based nanocomposites after 1 and
794 5 storage weeks. The moisture content of the PVA film was (6.3±0.1) % and (6.5±0.1) % after 1 or
795 5 weeks of storage, respectively, which indicates that equilibrium was reached after only 1 week of
796 storage (Cano et al., 2015). Moreover, the PVA film exhibited higher values than the PVA_CH
797 films due to the higher hydrophilic nature of PVA (Fortunati et al., 2013; Kavoosi et al., 2014).
798 PVA matrix is soluble in deionized water whereas chitosan is soluble in acid solution (1 v/v% of
799 glacial acetic acid); as a consequence, the PVA exhibited a higher humidity affinity respect to
800 PVA_CH film. The reduction of the moisture content in PVA_CH reinforced with CNC extracted
801 from straw and husk can be justified considering the barrier effect that CNC are able to induced in a
802 polymeric matrix (Fortunati et al., 2012; Peresin et al., 2010). At the end of the storage time (5

weeks), the moisture content tended to decrease respect to the values obtained after 1 week of storage for different systems, due to some aging phenomena of the materials (Peresin et al., 2010). Finally, the effectiveness of the developed active films as potential systems for industrial applications packaging was evaluated by visual observation of the fungal growth inhibition on food samples induced by chitosan or the combination of chitosan with different typologies and contents of CNC in PVA matrix. Figure 8 shows the appearance of sliced prunes at day 0 and after several days. In the case of prunes in contact with the neat PVA film, a rapid growth of the fungi was observed just after 4 days and became more evidently after 1 week of treatment, whereas no fungal growth was observed for prunes in contact with PVA_CH film until 10 days at room temperature. This proves the efficacy of chitosan against the microorganism development. A similar behavior was also observed for the PVA_CH based formulations reinforced with a 1 wt% of different CNC, with a first fungal growth detected after 7 days of incubation, although any positive effect of CNC addition at this low content was detected with respect to the PVA_CH blend. On the other hand, an incredible effect of CNC_{husk_enz} and CNC_{straw_enz} addition at 3 wt% to the PVA_CH blend was observed since the ternary formulation preserved the prunes till the 20^{th} day of storage. However, just after few days of storage prunes presented a clear physical deterioration and a loss of their organoleptic properties due to the experimental storage conditions (room temperature, uncontrolled atmosphere); in any case it is important to highlight that for ternary systems with 3 wt% of CNC, microbial growth was not observed until the end of the study (20 days). Specific isolation and characterization of fungal species observed on slides prunes were carried out. The fungi (air-borne spores) resulted identified as *Penicillium (ex. P. expansum*) and *Aspergillus* (*A. niger*) spp. that, as typical saprophytes, occurred frequently during post-harvest, causing damages by soft skinned on fresh fruits, like plum (Toma and Rajab, 2014).

4. Conclusions

828 Cellulose nanocrystals were here successfully extracted from both barley straw and husk by
829 applying and comparing, for the first time for these agricultural residues, two different approaches:
830 a chemical alkaline and an enzymatic pre-treatment. Furthermore, an acidic hydrolysis was
831 performed for the isolation of CNC. The results evidenced the major effectiveness of the enzymatic
832 pre-treatment on the quality of obtained CNC; nevertheless, all the different typologies of isolated
833 nanocrystals were added to the poly(vinyl alcohol) (PVA)_natural chitosan (CH) blends and some
834 different characterizations were carried out to evaluate the potential use of CNC as reinforcement
835 phases in new nanocomposites formulations for industrial applications. The results indicated that
836 chitosan reduced the optical transparency and the mechanical response of PVA matrix, whereas the
837 combination of chitosan with CNC (especially when extracted by enzymatic treatment and added at
838 a higher content) was able to positively modulate the optical properties, the mechanical and thermal
839 responses. In particular, the results of mechanical characterization, of interest for the final
840 application at an industrial level of the proposed systems, underlined that, even if the presence of
841 the chitosan, selected for its potential antimicrobial properties, can negatively compromise the
842 mechanical response of PVA in terms of deformability (that represents the most important
843 mechanical property for a packaging film), the addition of a very low content of a bio-based/natural
844 nanofiller as CNC to the selected biodegradable matrices, can positively counterbalance the final
845 mechanical response of PVA_CH blend, with a right compromise between elastic and plastic
846 response of the film, useful for the final practical application.
847 Finally, focusing on a possible practical application of the proposed formulations as novel package
848 solutions, the results from the overall migration test underlined that the migration levels, into food
849 simulants, were well below the permitted limits by the current legislation, while the food-contact
850 test evidenced the effectiveness of the proposed formulations to improve the shelf-life and quality
851 of perishable food products, such as prunes. The antibacterial assays also underlined the positive
852 performance of the nanocomposite films in the growth inhibition of two different plant and fruit
853 bacterial pathogens.

In conclusion, the results here presented suggest the potentiality of using the developed biodegradable films reinforced with a bio-based filler extracted from agricultural residues in some specific industrial sectors as, for example, the active packaging field here demonstrated, and the biomedicine and tissue engineering sectors where a combination of mechanical performances and antimicrobial response are strongly required.

860 **References**

861 Abdelrazek, E. M., Elashmawi, I. S., Labeeb, S., 2010. Chitosan filler effects on the experimental
862 characterization, spectroscopic investigation and thermal studies of PVA/PVP blend films. Physica
863 B: Cond. Matter 405(8), 2021-2027.

864 Abraham, R. E., Vongsvivut, J., Barrow, C. J., Puri, M., 2015. Understanding physicochemical
865 changes in pretreated and enzyme hydrolysed hemp (Cannabis sativa) biomass for biorefinery
866 development. Biomass Conv. Biorefi.1-12.

867 Adapa, P., Tabil, L., Schoenau, G., 2009. Compaction characteristics of barley, canola, oat and
868 wheat straw. Biosystems Eng. 104(3), 335-344.

869 Alemdar, A., Sain, M., 2008. Isolation and characterization of nanofibers from agricultural
870 residues–Wheat straw and soy hulls. Bioresource Technol. 99(6), 1664-1671.

871 Amer, A. A., El Maghraby, A., Malash, G. F., Nahla, T. A., 2007. Extensive characterization of raw
872 barley straw and study the effect of steam pretreatment. J. Appl. Res. Sci. 3, 1336-1342

873 Ang, T. N., Ngoh, G. C., Chua, A. S. M., Lee, M. G., 2012. Elucidation of the effect of ionic liquid
874 pretreatment on rice husk via structural analyses. Biotechnol. Biofuel. 5(1), 1.

875 Azizul, H. M., Kang, T. H., Kim, J. H., Yun, H. D., 2012. Effect of dilute alkali on structural
876 features and enzymatic hydrolysis of barley straw (Hordeum vulgare) at boiling temperature with
877 low residence time. J. Microbiol. Biotechnol. 22(12), 1681-1691.

878 Bahrami, S. B., Kordestani, S. S., Mirzadeh, H., Mansoori, P., 2003. Poly (vinyl alcohol)-chitosan
879 blends: preparation, mechanical and physical properties. Iran. Polym. J. 12, 139-146.

880 Besbes, I., Alila, S., Boufi, S., 2011. Nanofibrillated cellulose from TEMPO-oxidized eucalyptus
881 fibres: effect of the carboxyl content. Carbohyd. Polym. 84(3), 975-983.

882 Bledzki, A. K., Mamun, A. A., Volk, J., 2010. Barley husk and coconut shell reinforced
883 polypropylene composites: the effect of fibre physical, chemical and surface properties. Composites
884 Sci. Technol. 70(5), 840-846.

885 Bondeson, D., Mathew, A., Oksman, K., 2006. Optimization of the isolation of nanocrystals from
886 microcrystalline cellulose by acid hydrolysis. Cellulose 13(2), 171-180.
887 Bonilla, J., Fortunati, E., Atares, L., Chiralt, A., Kenny, J. M., 2014. Physical, structural and
888 antimicrobial properties of poly vinyl alcohol-chitosan biodegradable films. Food Hydrocolloid. 35,
889 463-470.
890 Bonilla, J., Fortunati, E., Atarés, L., Chiralt, A., Kenny, J. M., 2014. Physical, structural and
891 antimicrobial properties of poly vinyl alcohol–chitosan biodegradable films. Food Hydrocolloid. 35,
892 463-470.
893 Bouasker, M., Belayachi, N., Hoxha, D., Al-Mukhtar, M., 2014. Physical characterization of natural
894 straw fibers as aggregates for construction materials applications. Materials 7(4), 3034-3048.
895 Bowyer, J. L., Stockmann, V. E. 2001. Agricultural residues: An exciting bio-based raw material
896 for the global panels industry. Forest Prod. J. 51(1), 10.
897 Briggs, D., 2012. Barley, Springer Science & Business Media. Chapter 1.
898 Bulletin OEPP/EPPO. 2006. Bulletin 36, 129-133.
899 Cano, A. I., Cháfer, M., Chiralt, A., González-Martínez, C., 2015. Physical and microstructural
900 properties of biodegradable films based on pea starch and PVA. J. Food Eng. 167, 59-64.
901 Chandel, A. K., Antunes, F. A. F., Silva, M. B., da Silva, S. S., 2013. Unraveling the structure of
902 sugarcane bagasse after soaking in concentrated aqueous ammonia (SCAA) and ethanol production
903 by Scheffersomyces (Pichia) stipitis. Biotechnol. Biofuel. 6(1), 1.
904 CIE, 1995. Industrial colour-difference evaluation. Technical report 116/1995 ed. Commission
905 Internationale de I'Eclairage Central Bureau, Wien, Austria.
906 Cozzolino, D., Degner, S., Eglinton, J. K., 2015. In situ study of water uptake by the seeds,
907 endosperm and husk of barley using infrared spectroscopy. Spectrochim. Acta Part A 150, 200-206.
908 de Campos, A., Correa, A. C., Cannella, D., de M Teixeira, E., Marconcini, J. M., Dufresne, A.,
909 Mattoso, L. H. C., Cassland, P., Sanadi, A. R., 2013. Obtaining nanofibers from curauá and

910 sugarcane bagasse fibers using enzymatic hydrolysis followed by sonication. Cellulose 20(3), 1491-
911 1500.
912 Dhar, P., Bhardwaj, U., Kumar, A., Katiyar, V., 2014. Cellulose nanocrystals: a potential nanofiller
913 for food packaging applications. Food addit. Packag. 197-239.
914 El Halal, S. L. M., Colussi, R., Deon, V. G., Pinto, V. Z., Villanova, F. A., Carreño, N. L. V., Dias,
915 A. R. G., da Rosa Zavareze, E., 2015. Films based on oxidized starch and cellulose from barley.
916 Carbohyd. Polym. 133, 644-653.
917 El Miri, N., Abdelouahdi, K., Zahouily, M., Fihri, A., Barakat, A., Solhy, A., El Achaby, M., 2015.
918 Bio-nanocomposite films based on cellulose nanocrystals filled polyvinyl alcohol/chitosan polymer
919 blend. J. Appl. Polym. Sci. 132(22).
920 Espino, E., Cakir, M., Domenek, S., Román-Gutiérrez, A. D., Belgacem, N., Bras, J., 2014.
921 Isolation and characterization of cellulose nanocrystals from industrial by-products of Agave
922 tequilana and barley. Ind. Crop. Prod. 62, 552-559.
923 European Commission 2011. Commission Regulation (EU) No. 10/2011 of 14 January 2011 on
924 plastic materials and articles intended to come into contact with food. Off J Eur Comm, 50, 1-89.
925 European Standard EN 1186-1: 2002- Materials and articles in contact with foodstuffs. Plastics.
926 Guide to the selection of conditions and test methods for overall migration.
927 Figueiredo, L., Moura, C., Pinto, L. F. V., Ferreira, F. C., Rodrigues, A., 2015. Processing and
928 Characterization of 3D Dense Chitosan Pieces, for Orthopedic Applications, by Adding Plasticizers.
929 Procedia Eng. 110, 175-182.
930 Fortunati, E., Armentano, I., Zhou, Q., Iannoni, A., Saino, E., Visai, L., Berglund, L. A., Kenny, J.
931 M., 2012. Multifunctional bionanocomposite films of poly(lactic acid), cellulose nanocrystals and
932 silver nanoparticles. Carbohyd. Polym. 87(2), 1596-1605.
933 Fortunati, E., Luzi, F., Dugo, L., Fanali, C., Tripodo, G., Santi, L., Kenny, J. M., Torre, L., Bernini,
934 R., 2016. Effect of hydroxytyrosol methyl carbonate on the thermal, migration and antioxidant
935 properties of PVA based films for active food packaging. Polym. Int. doi: 10.1002/pi.5090.

936 Fortunati, E., Luzi, F., Puglia, D., Dominici, F., Santulli, C., Kenny, J. M., Torre, L., 2014.
937 Investigation of thermo-mechanical, chemical and degradative properties of PLA-limonene films
938 reinforced with cellulose nanocrystals extracted from Phormium tenax leaves. Eur. Polym. J. 56(0),
939 77-91.
940 Fortunati, E., Luzi, F., Puglia, D., Petrucci, R., Kenny, J. M., Torre, L., 2015. Processing of PLA
941 nanocomposites with cellulose nanocrystals extracted from Posidonia oceanica waste: Innovative
942 reuse of coastal plant. Ind. Crop. Prod. 67, 439-447.
943 Fortunati, E., Peltzer, M., Armentano, I., Torre, L., Jimenez, A., Kenny, J. M., 2012. Effects of
944 modified cellulose nanocrystals on the barrier and migration properties of PLA nano-biocomposites.
945 Carbohyd. Polym. 90(2), 948-956.
946 Fortunati, E., Puglia, D., Luzi, F., Santulli, C., Kenny, J. M., Torre, L., 2013. Binary PVA bio-
947 nanocomposites containing cellulose nanocrystals extracted from different natural sources: Part I.
948 Carbohyd. Polym. 97(2), 825-836.
949 Fortunati, E., Puglia, D., Monti, M., Peponi, L., Santulli, C., Kenny, J. M., Torre, L. 2013.
950 Extraction of Cellulose Nanocrystals from Phormium tenax Fibres. J. Polym. Env. 21(2), 319-328.
951 Fortunati, E., Puglia, D., Monti, M., Santulli, C., Maniruzzaman, M., Kenny, J. M., 2013. Cellulose
952 nanocrystals extracted from okra fibers in PVA nanocomposites. J. Appl. Polym. Sci. 128(5), 3220-
953 3230.
954 Hemalatha, K. S., Rukmani, K., Suriyamurthy, N., Nagabhushana, B. M., 2014. Synthesis,
955 characterization and optical properties of hybrid PVA–ZnO nanocomposite: A composition
956 dependent study. Mater. Res. Bull. 51, 438-446.
957 Hendriks, A., Zeeman, G., 2009. Pretreatments to enhance the digestibility of lignocellulosic
958 biomass. Bioresource Technol. 100(1), 10-18.
959 Henrique, M. A., Silvério, H. A., Neto, W. P. F., Pasquini, D. 2013. Valorization of an agro-
960 industrial waste, mango seed, by the extraction and characterization of its cellulose nanocrystals. J.
961 Environ. Manag. 121, 202-209.

962 Jacobsen, S. E., Wyman, C. E., 2002. Xylose monomer and oligomer yields for uncatalyzed
963 hydrolysis of sugarcane bagasse hemicellulose at varying solids concentration. Ind. Eng. Chem.
964 Res. 41(6), 1454-1461.
965 Johar, N., Ahmad, I., Dufresne, A., 2012. Extraction, preparation and characterization of cellulose
966 fibres and nanocrystals from rice husk. Ind. Crop. Prod. 37(1), 93-99.
967 Kanatt, S. R., Rao, M. S., Chawla, S. P., Sharma, A., 2012. Active chitosan–polyvinyl alcohol films
968 with natural extracts. Food Hydrocolloid. 29(2), 290-297.
969 Kavoosi, G., Nateghpoor, B., Dadfar, S. M. M., Dadfar, S. M. A., 2014. Antioxidant, antifungal,
970 water binding, and mechanical properties of poly (vinyl alcohol) film incorporated with essential oil
971 as a potential wound dressing material. J. Appl. Polym. Sci. 131(20).
972 Khan, A., Huq, T., Khan, R. A., Riedl, B., Lacroix, M., 2014. Nanocellulose-based composites and
973 bioactive agents for food packaging. Crit. Rev. Food Sci. 54(2), 163-174.
974 Khan, A., Khan, R. A., Salmieri, S., Le Tien, C., Riedl, B., Bouchard, J., Chauve, G., Tan, V.,
975 Kamal, M. R., Lacroix, M., 2012. Mechanical and barrier properties of nanocrystalline cellulose
976 reinforced chitosan based nanocomposite films. Carbohyd. Polym., 90(4), 1601-1608.
977 Kim, T. H., Taylor, F., Hicks, K. B., 2008. Bioethanol production from barley hull using SAA
978 (soaking in aqueous ammonia) pretreatment. Bioresource Technol., 99(13), 5694-5702.
979 Kjeldahl, J., 1883. A new method for the estimation of nitrogen in organic compounds. Z. Anal.
980 Chem, 22(1), 366.
981 Korte, S., Staiger, M. P., 2008. Effect of processing route on the composition and properties of
982 hemp fibre. Fibers Polym., 9, (5), 593-603.
983 Kristensen, J. B., Thygesen, L. G., Felby, C., Jørgensen, H., Elder, T., 2008. Cell-wall structural
984 changes in wheat straw pretreated for bioethanol production. Biotechnol. biofuel., 1(1), 1.
985 Lee, Y. M., Kimt, S. H., Kimt, S. J., 1996. Preparation and characteristics of β-chitin and poly
986 (vinyl alcohol) blend. Polymer 37(26), 5897-5905.

987 Li, D., Zhu, F. Z., Li, J. Y., Na, P., Wang, N., 2012. Preparation and characterization of cellulose
988 fibers from corn straw as natural oil sorbents. Ind. Eng. Chem. Res. 52(1), 516-524.
989 Li, F., Biagioni, P., Finazzi, M., Tavazzi, S., Piergiovanni, L., 2013. Tunable green oxygen barrier
990 through layer-by-layer self-assembly of chitosan and cellulose nanocrystals. Carbohyd. Polym.
991 92(2), 2128-2134.
992 Li, F., Mascheroni, E., Piergiovanni, L., 2015. The potential of nanocellulose in the packaging field:
993 a review. Packag. Technol. Sci. 28(6), 475-508.
994 Li, H.-Z., Chen, S.-C., Wang, Y.-Z., 2015. Preparation and characterization of nanocomposites of
995 polyvinyl alcohol/cellulose nanowhiskers/chitosan. Compos. Sci. Technol. 115, 60-65.
996 Li, Y., Pickering, K.L., 2008. Hemp fibre reinforced composites using chelator and enzyme
997 treatments. Compos. Sci. Technol., 68, 3293–3298.
998 Lu, P., Hsieh, Y.-L., 2012a. Cellulose isolation and core–shell nanostructures of cellulose
999 nanocrystals from chardonnay grape skins. Carbohyd. Polym. 87(4), 2546-2553.
1000 Lu, P., & Hsieh, Y.-L. (2012b). Preparation and characterization of cellulose nanocrystals from rice
1001 straw. Carbohyd. Polym. 87(1), 564-573.
1002 Luzi, F., Fortunati, E., Jiménez, A., Puglia, D., Pezzolla, D., Gigliotti, G., Kenny, J. M., Chiralt, A.,
1003 Torre, L., 2016. Production and characterization of PLA_PBS biodegradable blends reinforced with
1004 cellulose nanocrystals extracted from hemp fibres. Ind. Crop. Prod.
1005 doi:10.1016/j.indcrop.2016.01.045.
1006 Luzi, F., Fortunati, E., Puglia, D., Lavorgna, M., Santulli, C., Kenny, J. M., Torre, L., 2014.
1007 Optimized extraction of cellulose nanocrystals from pristine and carded hemp fibres. Ind. Crop.
1008 Prod. 56(0), 175-186.
1009 Mamun, A. A., Bledzki, A. K., 2014. Enzyme Modification of Grain By- products and Their
1010 Biocomposites: Characterization, Mechanical and Thermal Properties. Macromol. Mater. Eng.
1011 299(2), 248-256.

1012 Mohammadinejad, R., Karimi, S., Iravani, S., Varma, R. S., 2016. Plant-derived nanostructures:
1013 types and applications. Green Chem. 18(1), 20-52.
1014 Mood, S. H., Golfeshan, A. H., Tabatabaei, M., Abbasalizadeh, S., Ardjmand, M. 2013.
1015 Comparison of different ionic liquids pretreatment for barley straw enzymatic saccharification. 3
1016 Biotec 3(5), 399-406.
1017 Nakano, Y., Bin, Y., Bando, M., Nakashima, T., Okuno, T., Kurosu, H., Matsuo, M. Structure and
1018 mechanical properties of chitosan/poly (vinyl alcohol) blend films. (Vol. 258, pp. 63-81): Wiley
1019 Online Library.
1020 Ouajai, S., Shanks, R. A., 2005. Morphology and structure of hemp fibre after bioscouring.
1021 Macromol. Biosci. 5(2), 124-134.
1022 Pakarinen, A., Zhang, J., Brock, T., Maijala, P., Viikari, L. 2012. Enzymatic accessibility of fiber
1023 hemp is enhanced by enzymatic or chemical removal of pectin. Bioresource Technol.107, 275-281.
1024 Palumbo, M., Avellaneda, J., Lacasta, A. M. 2015. Availability of crop by-products in Spain: new
1025 raw materials for natural thermal insulation. Resour. Conserv. Recy. 99, 1-6.
1026 Palumbo, M., Formosa, J., Lacasta, A. M. 2015. Thermal degradation and fire behaviour of thermal
1027 insulation materials based on food crop by-products. Constr. Build. Mater. 79, 34-39.
1028 Peresin, M. S., Habibi, Y., Vesterinen, A.-H., Rojas, O. J., Pawlak, J. J., Seppälä, J. V., 2010. Effect
1029 of moisture on electrospun nanofiber composites of poly (vinyl alcohol) and cellulose nanocrystals.
1030 Biomacromolecules 11(9), 2471-2477.
1031 Raj, T., Kapoor, M., Gaur, R., Christopher, J., Lamba, B., Tuli, D. K., Kumar, R., 2015. Physical
1032 and chemical characterization of various Indian agriculture residues for biofuels production. Ener.
1033 Fuel. 29(5), 3111-3118.
1034 Reddy, N., Yang, Y., 2005. Properties and potential applications of natural cellulose fibers from
1035 cornhusks. Green Chem. 7(4), 190-195.
1036 Reddy, N., Yang, Y., 2009. Natural cellulose fibers from soybean straw. Bioresource Technol.
1037 100(14), 3593-3598.

1038 Ricciardi, R., Auriemma, F., De Rosa, C., Lauprêtre, F., 2004. X-ray diffraction analysis of poly
1039 (vinyl alcohol) hydrogels, obtained by freezing and thawing techniques. Macromolecules 37(5),
1040 1921-1927.
1041 Rinaudo, M., 2006. Chitin and chitosan: properties and applications. Prog. Polym. Sci. 31(7), 603-
1042 632.
1043 Roman, M., Winter, W. T., 2004. Effect of sulfate groups from sulfuric acid hydrolysis on the
1044 thermal degradation behavior of bacterial cellulose. Biomacromolecules 5(5), 1671-1677.
1045 Roohani, M., Habibi, Y., Belgacem, N. M., Ebrahim, G., Karimi, A. N., Dufresne, A., 2008.
1046 Cellulose whiskers reinforced polyvinyl alcohol copolymers nanocomposites. Eur. Polym. J. 44(8),
1047 2489-2498.
1048 Schaad, N. W., Jones, J. B., Chun, W., 1988. Laboratory guide for identification of plant pathogenic
1049 bacteria. APS press St. Paul, MN.
1050 Singh, J., 2015. Overview of electric power potential of surplus agricultural biomass from
1051 economic, social, environmental and technical perspective—A case study of Punjab. Renew. Sust.
1052 Energ. Rev. 42, 286-297.
1053 Singh, S., Cheng, G., Sathitsuksanoh, N., Wu, D., Varanasi, P., George, A., Balan, V., Gao, X.,
1054 Kumar, R., Dale, B. E., 2015. Comparison of different biomass pretreatment techniques and their
1055 impact on chemistry and structure. Front Energy Res. 2, 62.
1056 Siqueira, G., Bras, J., Dufresne, A., 2010. Cellulosic bionanocomposites: a review of preparation,
1057 properties and applications. Polymers, 2(4), 728-765.
1058 Steel, R. G. D., Jh Dickey, D. A., 1997. Principles and procedures of statistics a biometrical
1059 approach. WCB/McGraw-Hill.
1060 Sun, J. X., Xu, F., Sun, X. F., Xiao, B., Sun, R. C., 2005. Physico-chemical and thermal
1061 characterization of cellulose from barley straw. Polym.Degrad. Stabil. 88(3), 521-531.

1062 Sun, R., Sun, X. F., Liu, G. Q., Fowler, P., Tomkinson, J. , 2002. Structural and physicochemical
1063 characterization of hemicelluloses isolated by alkaline peroxide from barley straw. Polym. Int.
1064 51(2), 117-124.
1065 Sun, X. F., Xu, F., Sun, R. C., Fowler, P., Baird, M. S., 2005. Characteristics of degraded cellulose
1066 obtained from steam-exploded wheat straw. Carbohyd. Res., 340(1), 97-106.
1067 Toma F.M., and Rajab N.N., (2014). Isolation and identification of fungi from dried fruits and study
1068 of quantitative estimation of aflatoxin. Zanco J Pure App Sci., 26(4), 49-60.
1069 Toth, I. K., Bell, K. S., Holeva, M. C., Birch, P. R. J., 2003. Soft rot erwiniae: from genes to
1070 genomes. Mol. plant pathol. 4(1), 17-30.
1071 Tripathi, S., Mehrotra, G. K., Dutta, P. K., 2009. Physicochemical and bioactivity of cross-linked
1072 chitosan–PVA film for food packaging applications. Int. J. Biol. Macromol. 45(4), 372-376.
1073 Van Soest P.J., 1963. Use of detergents in the analysis fibrous feeds. I. Preparation of fiber resi-
1074 dues of low nitrogen content. J. Assoc. Off. Anal. Chem, 46, 825-835.
1075 Wang, H.M., Postle, R., Kessler, R.W., Kessler, W., 2003. Removing pectin and lignin during
1076 chemical processing of hemp for textile applications. Textile Res J., 73, 664-669.
1077 Wang, S., Marcone, M. F., Barbut, S., Lim, L.-T., 2012. Fortification of dietary biopolymers-based
1078 packaging material with bioactive plant extracts. Food Res. Int. 49(1), 80-91.
1079 Wessén, B., Berg, B., 1986. Long-term decomposition of barley straw: chemical changes and
1080 ingrowth of fungal mycelium. Soil Biol. Biochem. 18(1), 53-59.
1081 Wiśniewska, S. K., Nalaskowski, J., Witka-Jeżewska, E., Hupka, J., Miller, J. D. (2003). Surface
1082 properties of barley straw. Colloid. Surface. B 29(2), 131-142.
1083 Zhang, W., He, X., Li, C., Zhang, X., Lu, C., Zhang, X., Deng, Y., 2014. High performance poly
1084 (vinyl alcohol)/cellulose nanocrystals nanocomposites manufactured by injection molding.
1085 Cellulose 21(1), 485-494.
1086

Figure and Table Captions

Scheme 1: Scheme of barley straw and husk chemical pre-treatments.

Figure 1: FESEM investigation of barley straw and husk. Straw raw material (surface (a) and fractured surface (insert)), straw chemically (b) and enzymatically pre-treated (c). Husk raw material (surface (d) and fractured surface (insert)), husk chemically (e) and enzimatically pre-treated (f).

Figure 2: Derivative curve (DTG) of straw raw material, chemically (a) and enzymatically (b) pre-treated and DTG of husk raw material, chemically (c) and enzymatically (d) pre-treated.

Figure 3: FESEM investigation of CNC_{straw_chem} (a), CNC_{straw_enz} (b), CNC_{husk_chem} (c), and CNC_{husk_enz} (d).

Figure 4: Panel A:FESEM investigation of fractured surface of PVA and PVA_CH based nanocomposites. Panel B: UV-Vis analysis of PVA and PVA_CH nanocomposites reinforced with 1% wt of CNC extracted from straw and husk chemically and enzimatically pretreated (a). UV-Vis analysis of PVA and PVA_CH nanocomposites reinforced with 1 and 3% wt of CNC_{straw_enz} and CNC_{husk_enz} (b).

Figure 5: X-ray diffraction (XRD) patterns of PVA, PVA_CH, PVA_CH_3CNC_{straw_enz} and PVA_CH_3 CNC_{husk_enz} (a). Stress-strain curves of PVA and PVA_CH based nanocomposites (b).

Figure 6: Overall migration in ethanol 10 (v/v)% and isooctane of PVA and PVA_CH based nanocomposites.

Figure 7: Appearance of fungal growth on sliced prunes after different times of storage coated with PVA and PVA_CH based nanocomposites at room temperature.

Figure 8: Antimicrobial properties of PVA and PVA_CH nanocomposites using *Xanthomonas arboricola* pv. *pruni* (Xap CFBP - 3894) and *Pectobacterium carotovorum* subsp. *odoriferum* (Pco - 1115) bacterial plant pathogens.

1112 **Table 1:** Composition of raw materials, cellulose content of the chemical and enzymatic pre-

1113 treatments and relative yields.

1114 **Table 2:** Colour coordinates of PVA and PVA_CH nanocomposites.

1115 **Table 3:** Thermal Properties of PVA and PVA_CH nanocomposites.

1116 **Table 4:** Mechanical properties of PVA and PVA_CH nanocomposites.

1117 **Table 5:** Moisture content (*MC*) of PVA and PVA_CH nanocomposites.

Table 1

Table 1: Composition of raw materials, cellulose content of the chemical and enzymatic pre-treatments and relative yields.

Raw materials				
	Straw		*Husk*	
Dry weight	93.2		90.8	
On the basis of dry weight				
Protein	2.6		6.4	
Ashes	10.5		6.0	
Lipids	2.0		3.5	
Others (fibres, derivatives, etc)	84.9		84.1	
Fibre composition of the raw materials (%)				
	Straw		*Husk*	
Cellulose	56.2		45.7	
Hemicellulose	7.0		22.4	
Lignin	9.2		7.2	
Others (pectins, lipids, proteins, sugars, organic acids)	7.6		24.7	
Cellulose content (%) after chemical and enzymatic pre-treatment				
	Straw		*Husk*	
	Chemical	*Enzymatic*	*Chemical*	*Enzymatic*
Cellulose	62.8	73.6	75.2	81.0
Cellulose purification fold with respect to raw materials	1.12	1.29	1.64	1.77
Cellulose yields (%) of chemical and enzymatic pre-treatment				
	Straw		*Husk*	
Chemical pre-treatment	45.0		50.0	
Enzymatic pre-treatment	36.6		30.0	

Table 2: Colour coordinates of PVA and PVA_CH nanocomposites.

Formulations	*L**	*a**	*b**	*ΔE**	*Gloss (°)*
PVA	99.10±0.04	-0.10±0.01	0.15±0.03	-	236±4
PVA_CH	98.85±0.09	-0.22±0.03	0.99±0.20	0.88	234±2
PVA_CH_1CNC$_{straw_chem}$	98.61±0.05	-0.18±0.01	1.06±0.06	1.04	228±2
PVA_CH_1CNC$_{straw_enz}$	98.29±0.10	-0.12±0.01	1.61±0.23	1.79	235±3
PVA_CH_1CNC$_{husk_chem}$	98.36±0.14	-0.19±0.02	1.24±0.23	1.35	233±2
PVA_CH_1CNC$_{husk_enz}$	98.52±0.04	-0.13±0.01	1.15±0.10	1.2	229±5
PVA_CH_3CNC$_{straw_enz}$	96.91±0.28	-0.08±0.02	4.45±0.62	4.82	230±4
PVA_CH_3CNC$_{husk_enz}$	98.07±0.21	-0.09±0.01	2.15±0.40	2.25	225±2

Table 3

Table 3: Thermal Properties of PVA and PVA_CH nanocomposites.

Formulations	*Cooling scan*				*Second heating scan*			
	T_g (°C)	ΔH_C (J/g)	T_C (°C)	X_C (%)	T_g (°C)	ΔH_m (J/g)	T_m (°C)	X_m (%)
PVA	72.8 ± 0.7	40.6 ± 2.8	191.3 ± 0.8	25.1 ± 1.7	79.6 ± 0.2	33.0 ± 0.9	216.9 ± 0.7	20.4 ± 0.6
PVA_CH	75.3 ± 0.2	28.9 ± 1.7	177.5 ± 0.8	16.1 ± 0.9	82.9 ± 0.7	34.3 ± 0.6	212.1 ± 0.9	19.1 ± 0.3
PVA_CH_1CNC$_{straw_chem}$	75.9 ± 0.7	28.3 ± 0.3	174.6 ± 1.3	15.6 ± 0.1	83.9 ± 0.4	28.5 ± 4.9	210.4 ± 0.3	15.7 ± 2.7
PVA_CH_1CNC$_{straw_enz}$	74.3 ± 0.7	29.7 ± 1.2	180.9 ± 1.4	16.5 ± 0.7	85.4 ± 0.3	32.7 ± 0.3	212.8 ± 0.2	18.0 ± 0.1
PVA_CH_1CNC$_{husk_chem}$	77.5 ± 1.1	32.0 ± 4.2	174.6 ± 1.3	17.6 ± 2.3	83.7 ± 0.5	33.7 ± 0.3	211.5 ± 1.3	18.6 ± 0.2
PVA_CH_1CNC$_{husk_enz}$	76.1 ± 0.9	29.4 ± 0.7	180.2±1.1	16.7 ± 0.4	80.9 ± 0.5	33.5 ± 1.7	213.3 ± 1.1	18.4 ± 0.9
PVA_CH_3CNC$_{straw_enz}$	75.5±0.4	32.8±0.4	177.4±0.6	18.3±0.2	81.3±0.1	31.4±0.6	213.4±0.2	17.2±0.3
PVA_CH_3CNC$_{husk_enz}$	77.6±0.9	29.8±0.6	177.2±1.1	16.9±0.3	82.0±0.4	34.1±0.9	213.4±0.2	18.8±0.5

Table 4

Table 4: Mechanical properties of PVA and PVA_CH nanocomposites.

Formulations	σ_B *(MPa)*	ε_B *(%)*	E_{Young} *(MPa)*
PVA	50.7 ± 6.9	225 ± 30	430 ± 60
PVA_CH	36.0 ± 9.5	110 ± 25	560 ± 40
PVA_CH_1CNC$_{straw_chem}$	47.4 ± 7.6	160 ± 20	680± 60
PVA_CH_1CNC$_{straw_enz}$	60.7 ± 8.1	220 ± 30	830± 65
PVA_CH_1CNC$_{husk_chem}$	62.5 ± 3.5	200 ± 25	830 ± 80
PVA_CH_1CNC$_{husk_enz}$	45.1 ± 2.5	180 ± 20	760 ± 60
PVA_CH_3CNC$_{straw_enz}$	64.9±7.0	190±20	1000±90
PVA_CH_3CNC$_{husk_enz}$	52.9±4.4	170±10	1160±200

Table 5

Table 5: Moisture content (*MC*) of PVA and PVA_CH nanocomposites.

Formulations	***MC (%)***	
	1th week	***5th week***
PVA	6.3 ± 0.5	6.5 ± 0.1
PVA_CH	6.1 ± 0.1	5.3 ± 0.1
PVA_CH_1CNC$_{straw_chem}$	5.1 ± 0.4	4.1 ± 0.1
PVA_CH_1CNC$_{straw_enz}$	5.8 ± 0.2	4.4 ± 0.2
PVA_CH_1CNC$_{husk_chem}$	5.6 ± 0.1	4.1 ± 0.7
PVA_CH_1CNC$_{husk_enz}$	4.3 ± 0.4	3.5 ± 0.1
PVA_CH_3CNC$_{straw_enz}$	4.2±0.3	3.2±0.3
PVA_CH_3CNC$_{husk_enz}$	3.8±0.3	2.5±0.1

Scheme 1

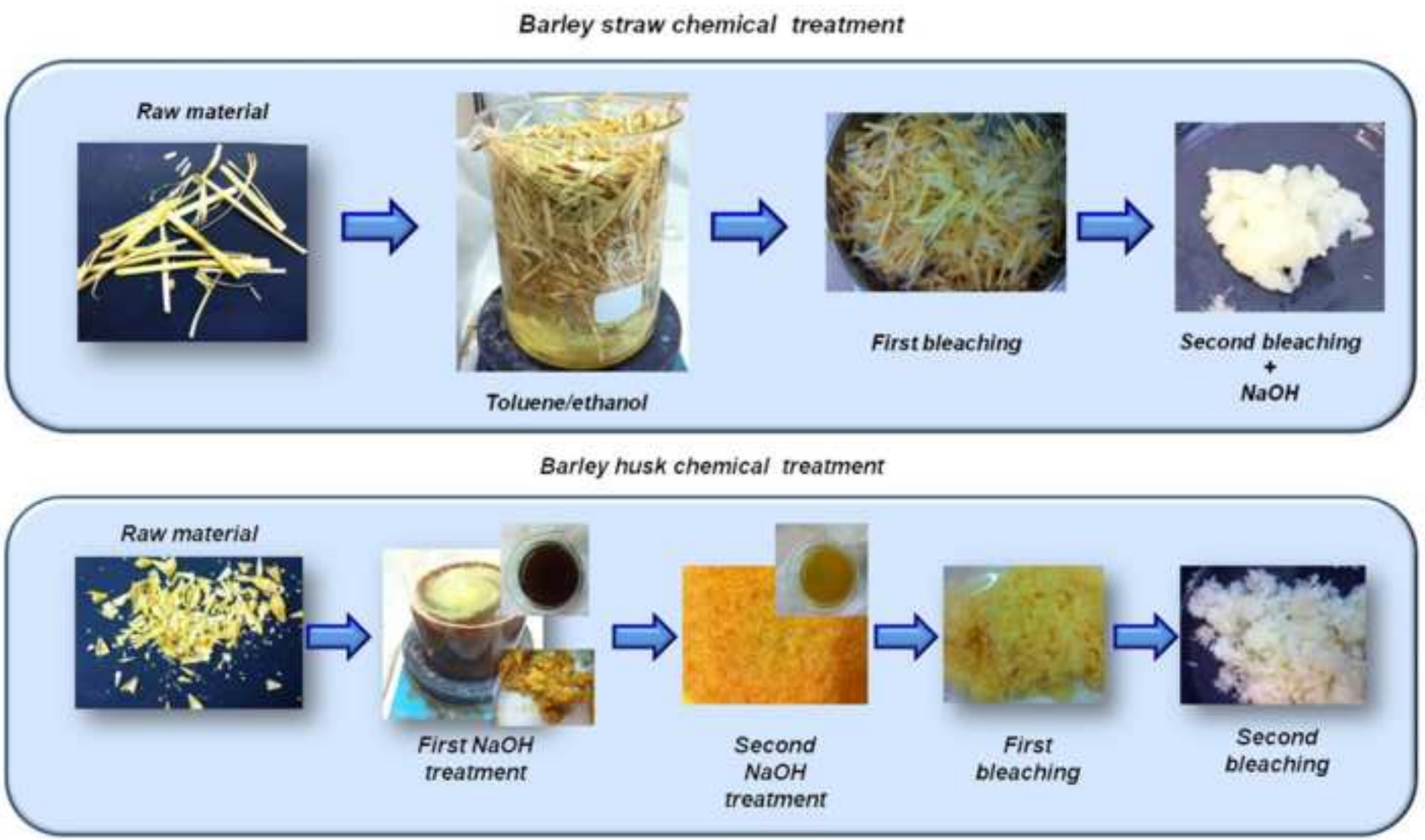
Barley straw chemical treatment
Raw material
Toluene/ethanol
First bleaching
Second bleaching
+
NaOH
Barley husk chemical treatment
Raw material
First NaOH
treatment
Second
NaOH
treatment
First
bleaching
Second
bleaching

Figure 1

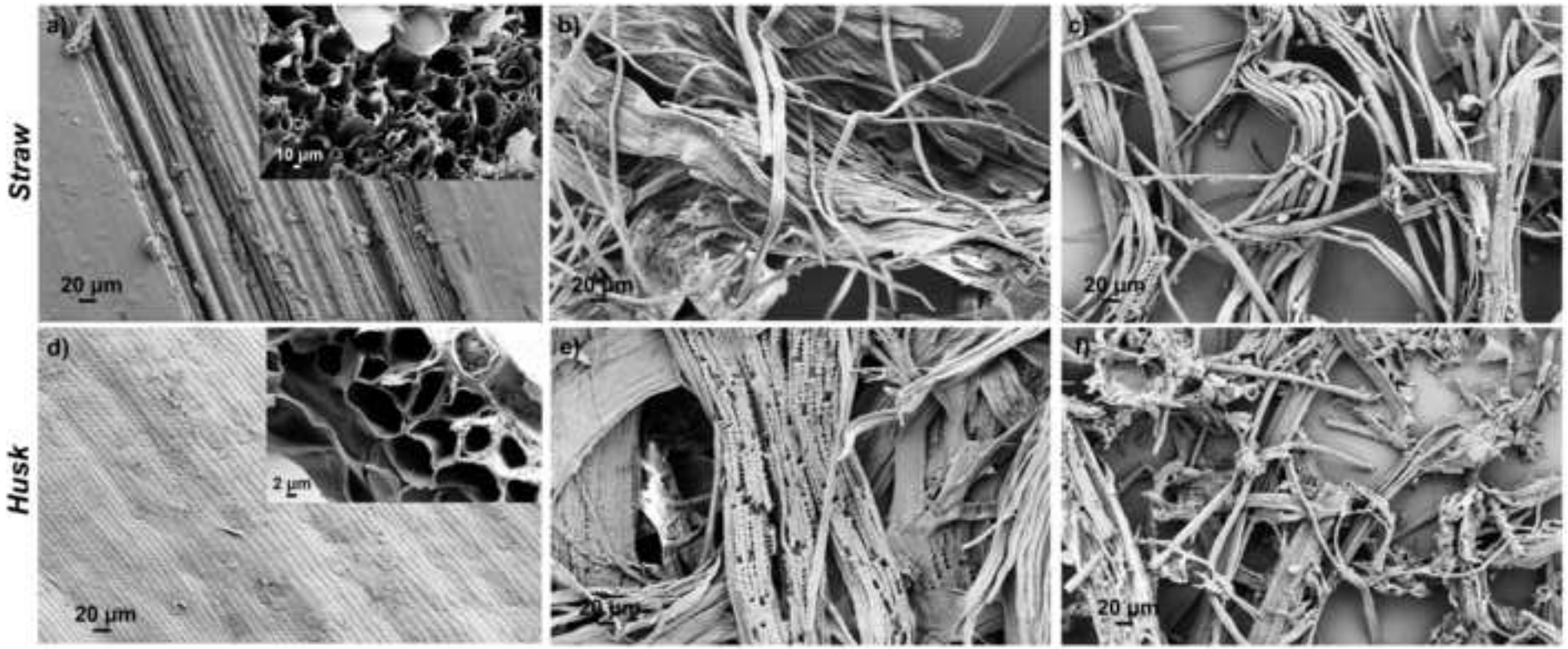

Figure 2

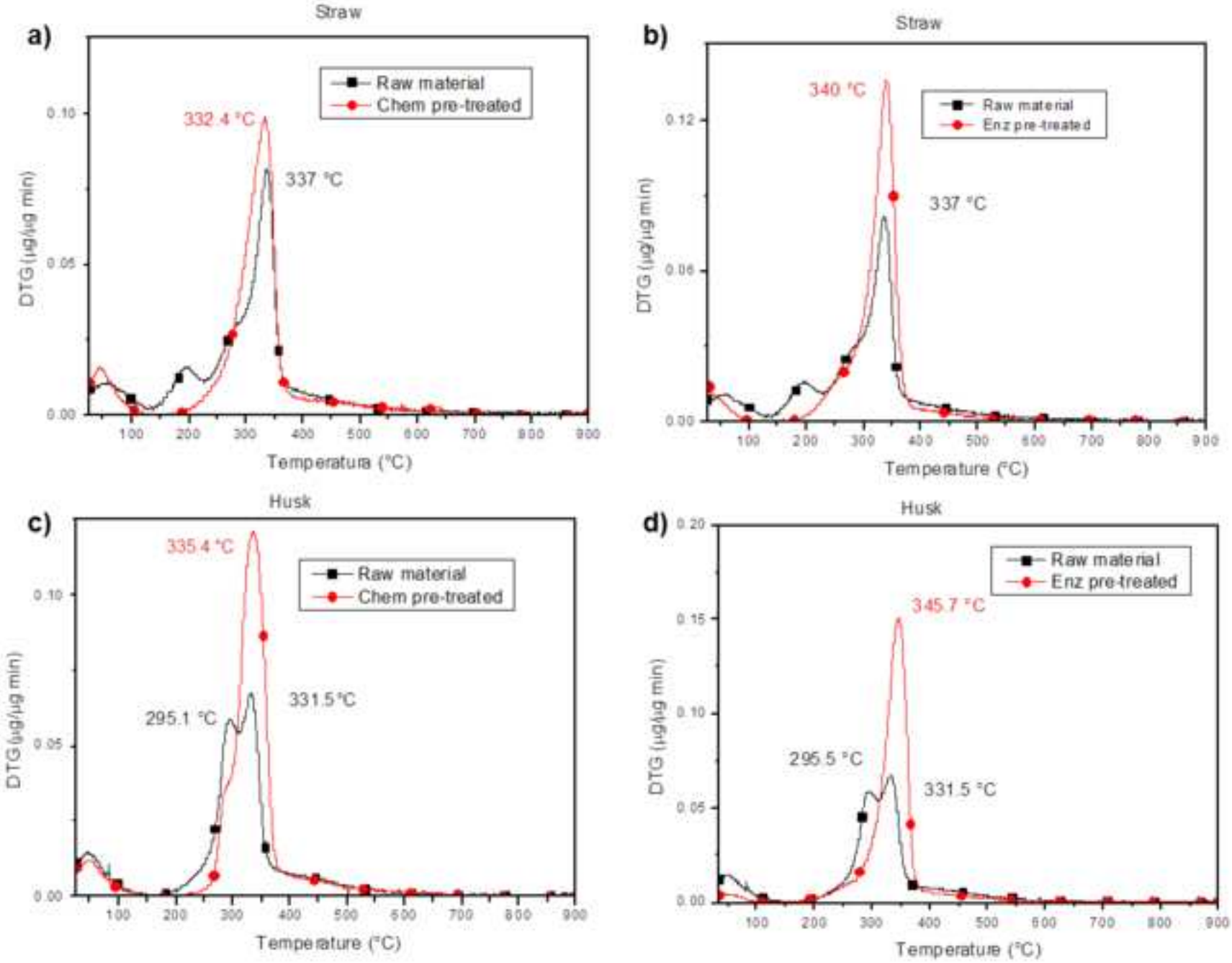
a)
Straw
Raw material
Chem pre-treated
332.4 °C
337 °C
DTG (µg/µg min)
Temperatura (°C)
b)
Straw
Raw material
Enz pre-treated
340 °C
337 °C
DTG (µg/µg min)
Temperature (°C)
c)
Husk
Raw material
Chem pre-treated
335.4 °C
295.1 °C
331.5 °C
DTG (µg/µg min)
Temperature (°C)
d)
Husk
Raw material
Enz pre-treated
345.7 °C
295.5 °C
331.5 °C
DTG (µg/µg min)
Temperature (°C)

Figure 3

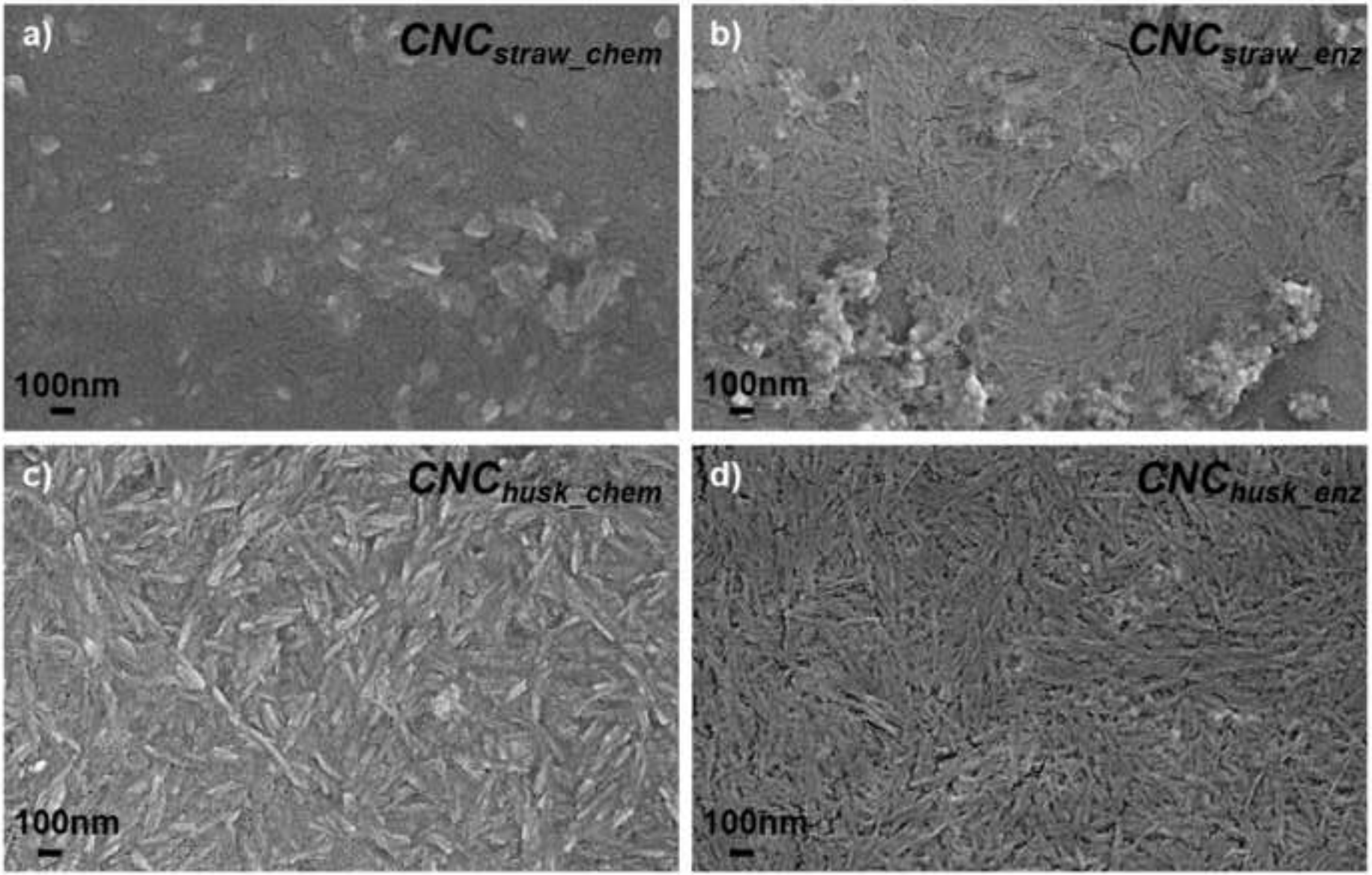
a)
CNC straw_chem
100nm
b)
CNC straw_enz
100nm
c)
CNC husk_chem
100nm
d)
CNC husk_enz
100nm

Figure 4

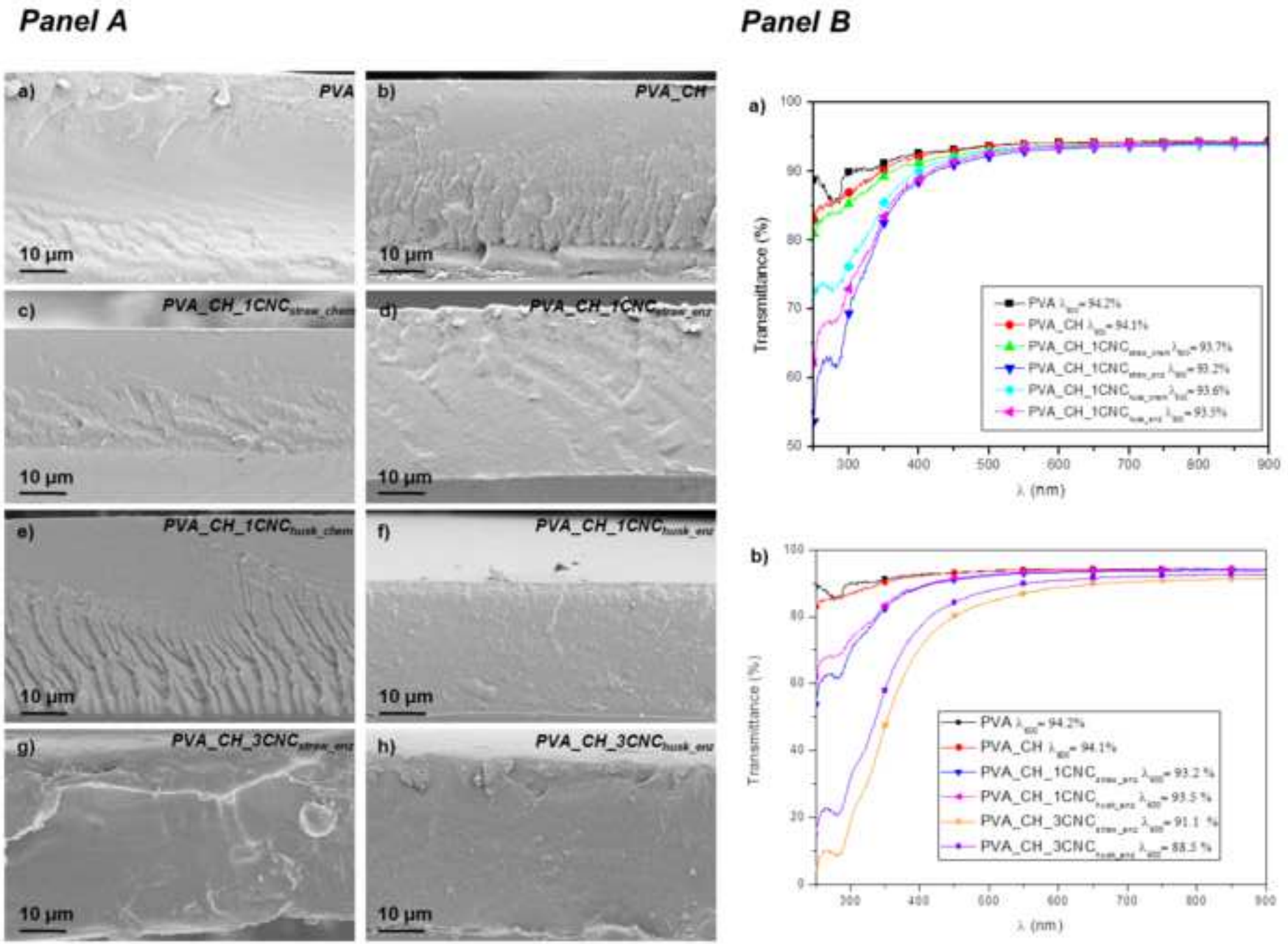
Panel A
a)
PVA
10 µm
b)
PVA_CH
10 µm
c)
PVA_CH_1CNC
10 µm
d)
PVA_CH_1CNC
10 µm
e)
PVA_CH_1CNC
10 µm
f)
PVA_CH_1CNC
10 µm
g)
PVA_CH_3CNC
10 µm
h)
PVA_CH_3CNC
10 µm
Panel B
a)
Transmittance (%)
λ (nm)
PVA
PVA_CH
PVA_CH_1CNC
PVA_CH_1CNC
PVA_CH_1CNC
PVA_CH_1CNC
b)
Transmittance (%)
λ (nm)
PVA
PVA_CH
PVA_CH_1CNC
PVA_CH_1CNC
PVA_CH_3CNC
PVA_CH_3CNC

Figure 5

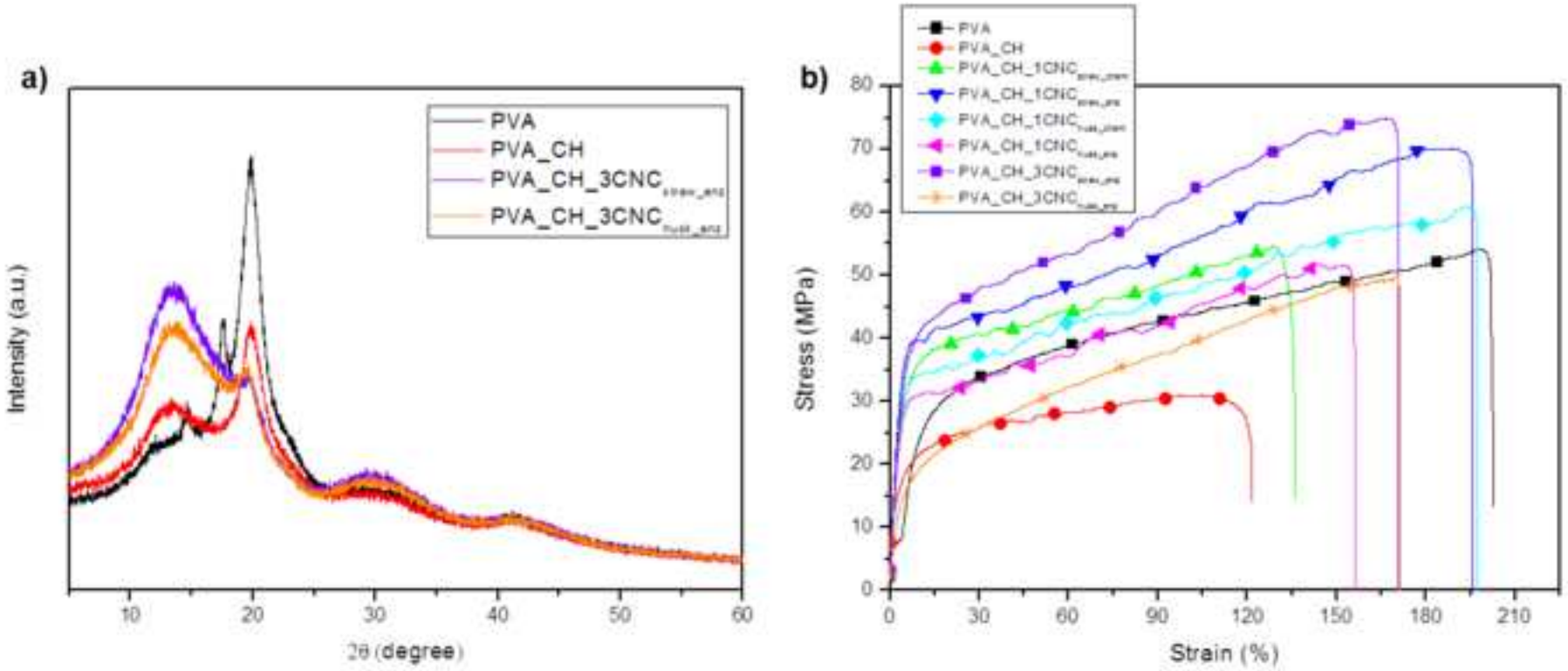
a)
PVA
PVA_CH
PVA_CH_3CNC
Intensity (a.u.)
10
20
30
40
50
60
2θ (degree)
b)
PVA
PVA_CH
PVA_CH_1CNC
PVA_CH_1CNC
PVA_CH_1CNC
PVA_CH_1CNC
PVA_CH_3CNC
PVA_CH_3CNC
Stress (MPa)
0
10
20
30
40
50
60
70
80
0
30
60
90
120
150
180
210
Strain (%)

Figure 6

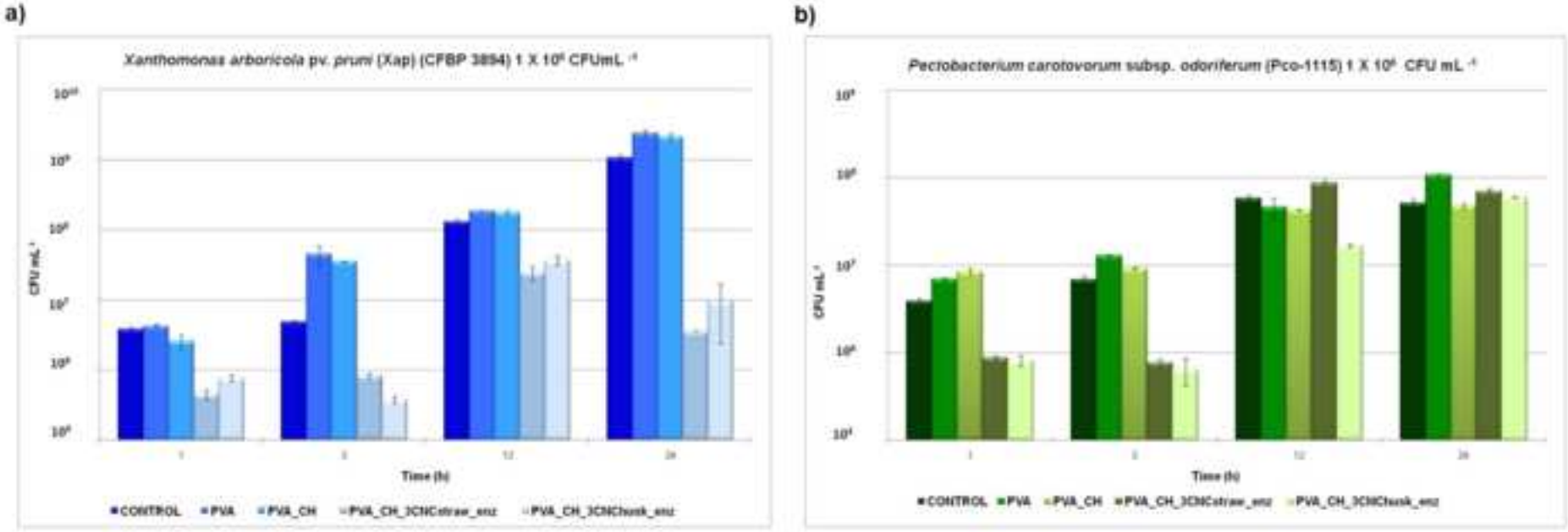
a)
Xanthomonas arboricola pv. pruni (Xap) (CFBP 3894) 1 X 10⁵ CFUmL⁻¹
CFU mL⁻¹
Time (h)
CONTROL
PVA
PVA_CH
PVA_CH_3CNCstraw_enz
PVA_CH_3CNChusk_enz
b)
Pectobacterium carotovorum subsp. odoriferum (Pco-1115) 1 X 10⁵ CFU mL⁻¹
CFU mL⁻¹
Time (h)
CONTROL
PVA
PVA_CH
PVA_CH_3CNCstraw_enz
PVA_CH_3CNChusk_enz

Figure 7

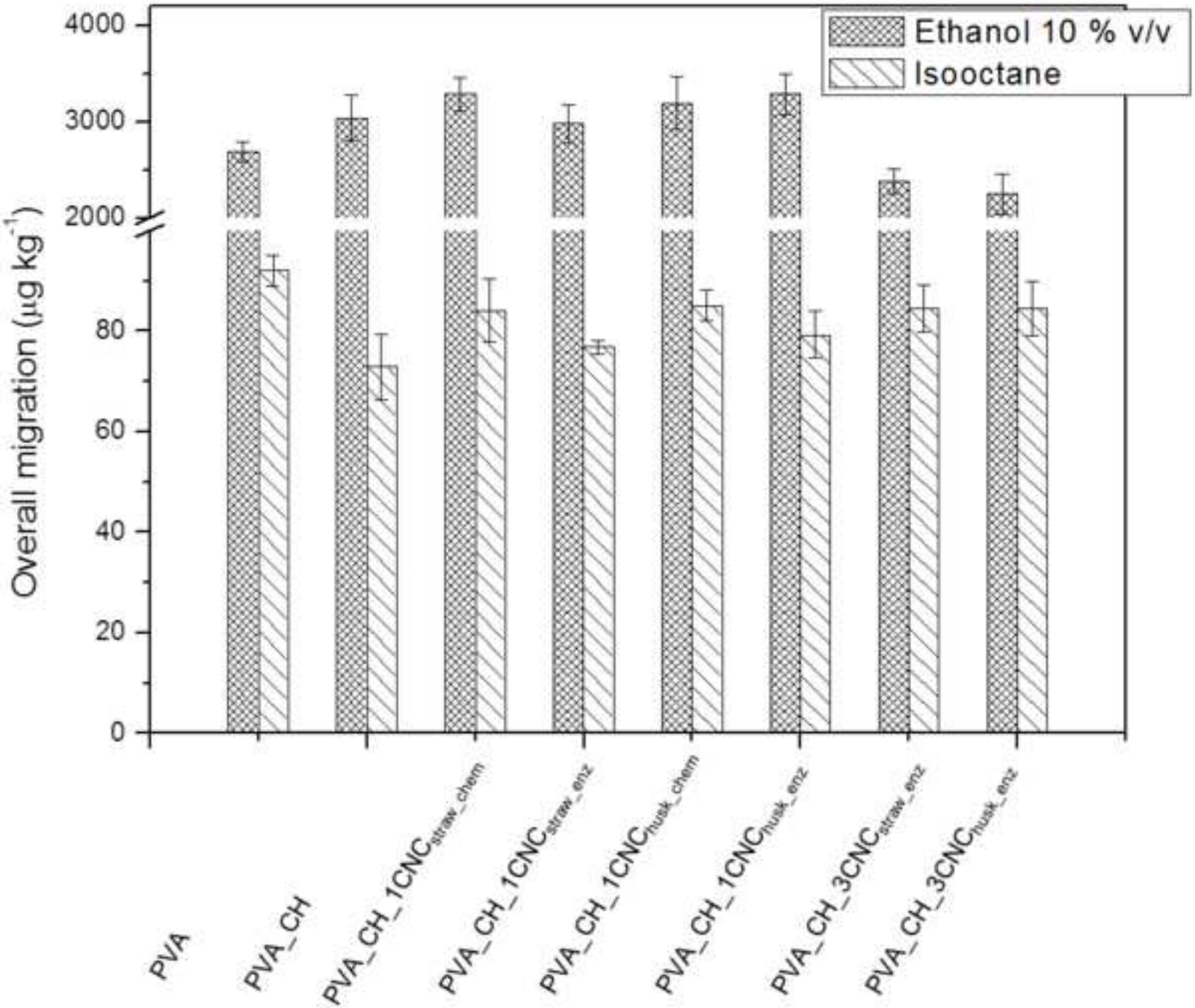
Ethanol 10 % v/v
Isooctane
Overall migration (μg kg-1)
4000
3000
2000
80
60
40
20
0
PVA
PVA_CH
PVA_CH_1CNCstraw_chem
PVA_CH_1CNCstraw_enz
PVA_CH_1CNChusk_chem
PVA_CH_1CNChusk_enz
PVA_CH_3CNCstraw_enz
PVA_CH_3CNChusk_enz

Figure 8

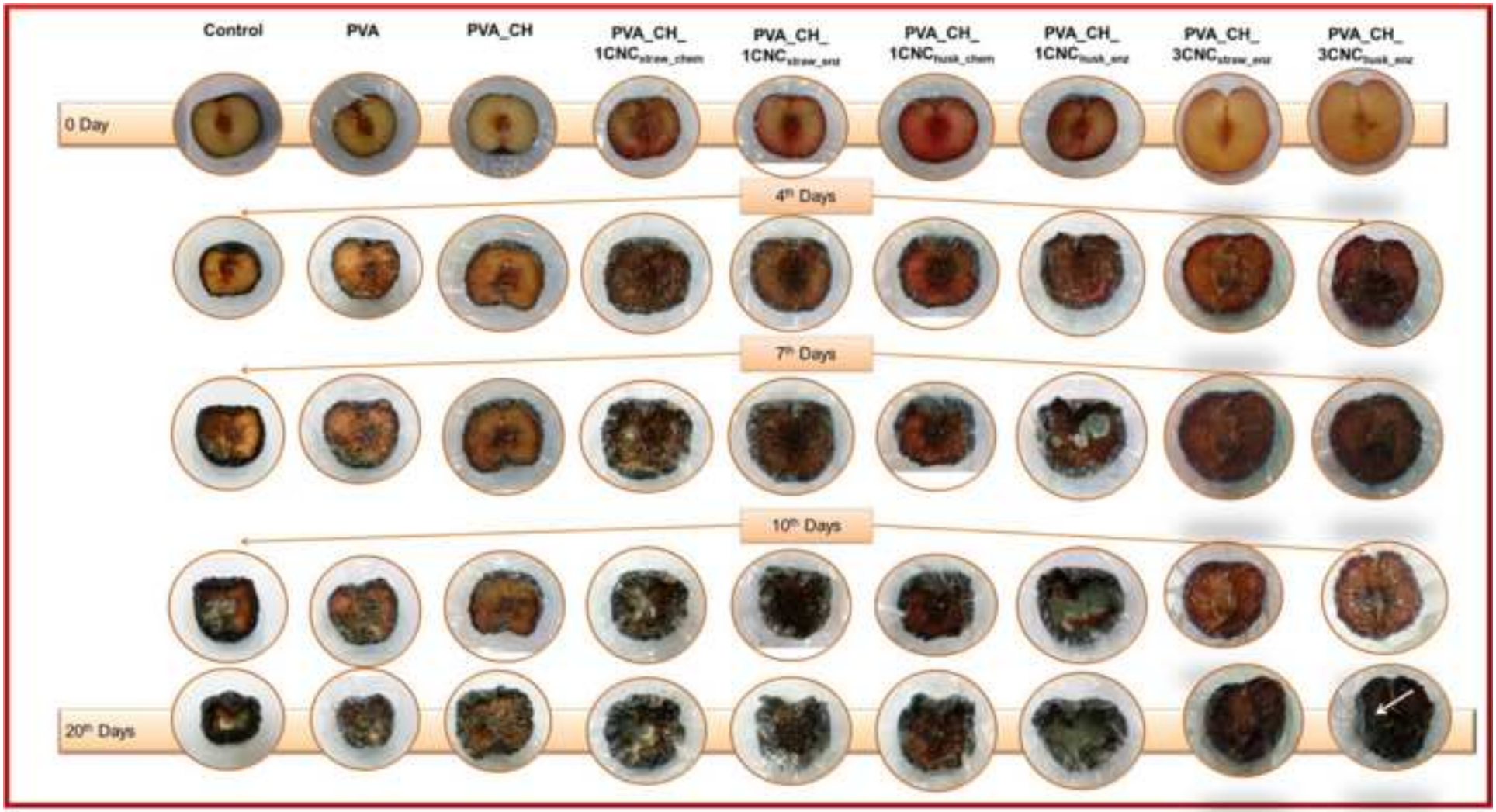
Control
PVA
PVA_CH
PVA_CH_ 1CNC straw_chem
PVA_CH_ 1CNC straw_enz
PVA_CH_ 1CNC husk_chem
PVA_CH_ 1CNC husk_enz
PVA_CH_ 3CNC straw_enz
PVA_CH_ 3CNC husk_enz
0 Day
4th Days
7th Days
10th Days
20th Days

Revalorization of barley straw and husk as precursors for cellulose nanocrystals extraction and their effect on PVA_CH nanocomposites

E. Fortunati[a*], P. Benincasa[b], G.M. Balestra[c], F. Luzi[a], A. Mazzaglia[c], D. Del Buono[b], D. Puglia[a], L. Torre[a]

[a]*University of Perugia, Civil and Environmental Engineering Department, UdR INSTM, Strada di Pentima 4, 05100 Terni (Italy)*

[b]*University of Perugia, Department of Agricultural, Food and Environmental Sciences, Borgo XX Giugno 74, 06121 Perugia (Italy)*

[c]*University of Tuscia, Department of Sciences for Agriculture and Forestry (DAFNE), Via S. Camillo de Lellis sns, 0100 Viterbo (Italy)*

[*]**Corresponding author**: Tel.: +39-0744492921; fax: +39-0744492950; E-mail address: elena.fortunati@unipg.it (E. Fortunati)

TABLE OF CONTENTS

Figure S1: FTIR analysis of raw material, chemically pre-treated and CNC from straw (a); raw material, enzimatically pre-treated and CNC from straw (b); raw material, chemically pre-treated and CNC from husk (c) and raw material, enzymatically pre-treated and CNC from husk (d).

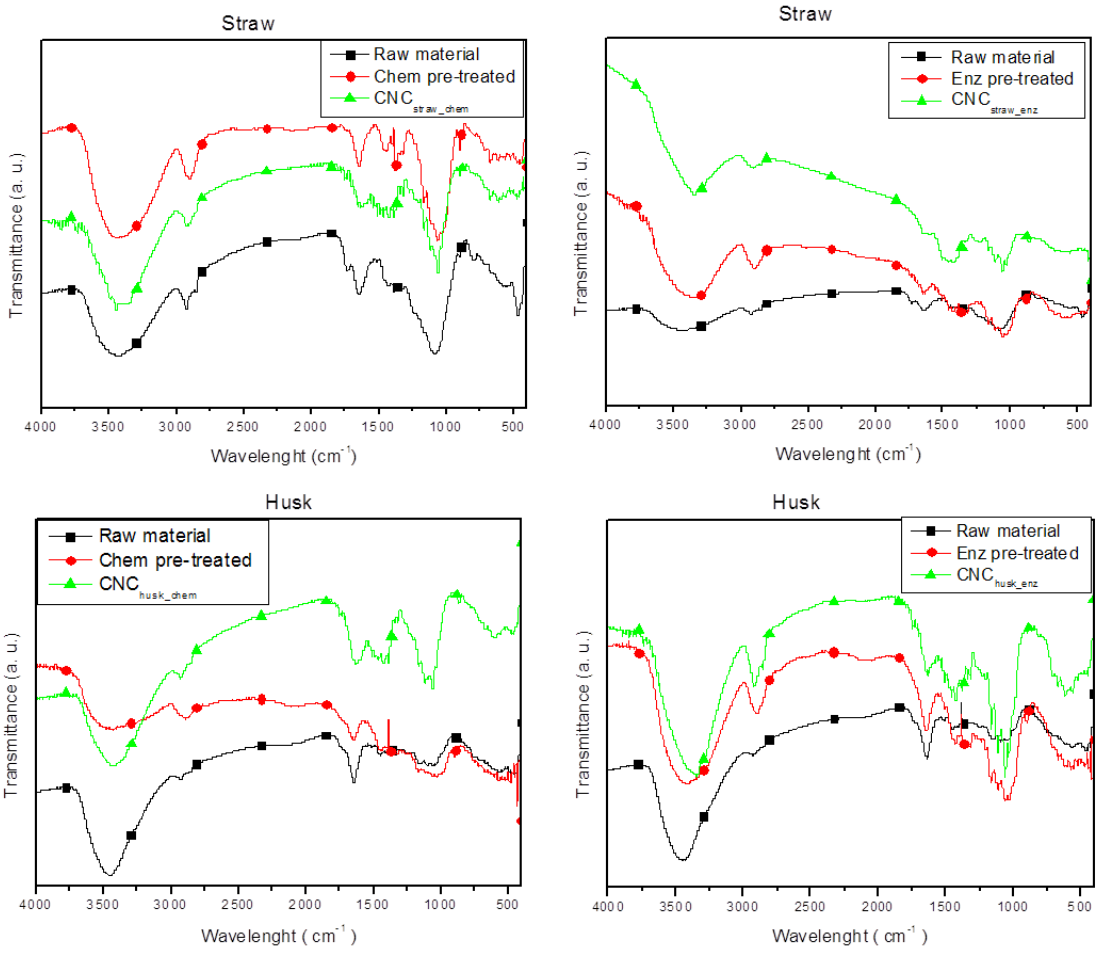

Figure S2: X-ray diffraction (XRD) patterns (a), and derivative curves (DTG) (b) of CNC_{straw_chem}, CNC_{straw_enz}, CNC_{husk_chem} and CNC_{husk_enz}. (inset: degradation temperature values).

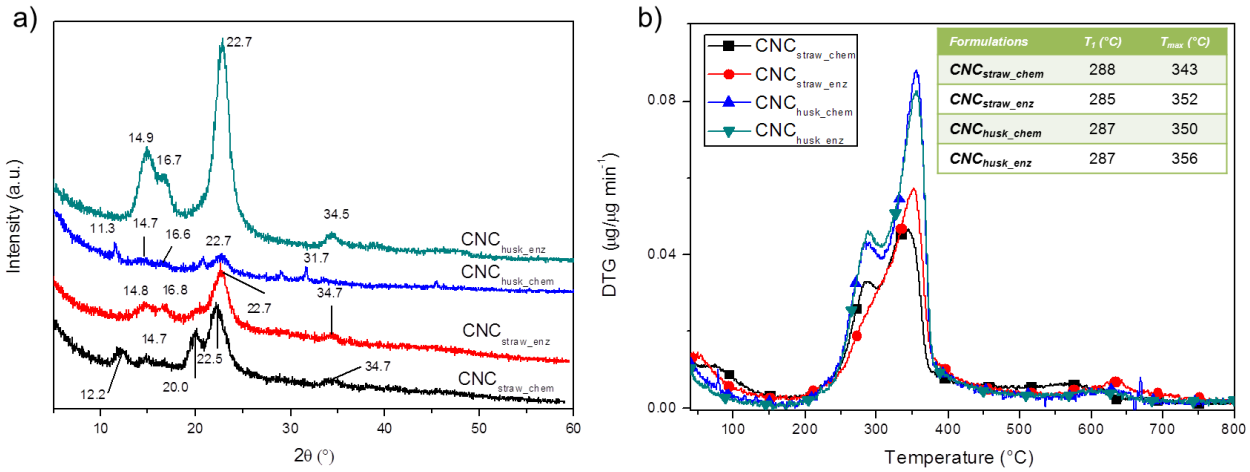

Table S1: Material formulations.

Formulations	**PVA (wt%)**	**CH (wt%)**	***CNC_{straw_chem}* (wt%)**	***CNC_{straw_enz}* (wt%)**	***CNC_{husk_chem}* (wt%)**	***CNC_{husk_enz}* (wt%)**
PVA	100	-	-	-	-	-
PVA_CH	90	10	-	-	-	-
PVA_CH_1CNC$_{straw_chem}$	89	10	1	-	-	-
PVA_CH_1CNC$_{straw_enz}$	89	10	-	1	-	-
PVA_CH_1CNC$_{husk_chem}$	89	10	-	-	1	-
PVA_CH_1CNC$_{husk_enz}$	89	10	-	-	-	1
PVA_CH_3CNC$_{straw_enz}$	87	10	-	-	3	-
PVA_CH_3CNC$_{husk_enz}$	87	10	-	-	-	3